*Cerebral Cortex*, April 2018;28: 1312–1328

**doi: 10.1093/cercor/bhx044**
Advance Access Publication Date: 10 March 2017
Original Article

ORIGINAL ARTICLE

# POm Thalamocortical Input Drives Layer-Specific Microcircuits in Somatosensory Cortex

Nicholas J. Audette, Joanna Urban-Ciecko, Megumi Matsushita and Alison L. Barth*

Department of Biological Sciences and Center for the Neural Basis of Cognition, Carnegie Mellon University, 4400 Fifth Avenue, Pittsburgh, PA 15213, USA

*Address correspondence to Alison L. Barth. Email: albarth@andrew.cmu.edu

## Abstract

Higher-order thalamic nuclei, such as the posterior medial nucleus (POm) in the somatosensory system or the pulvinar in the visual system, densely innervate the cortex and can influence perception and plasticity. To systematically evaluate how higher-order thalamic nuclei can drive cortical circuits, we investigated cell-type selective responses to POm stimulation in mouse primary somatosensory (barrel) cortex, using genetically targeted whole-cell recordings in acute brain slices. We find that ChR2-evoked thalamic input selectively targets specific cell types in the neocortex, revealing layer-specific modules for the summation and processing of POm input. Evoked activity in pyramidal neurons from deep layers is fast and synchronized by rapid feedforward inhibition from GABAergic parvalbumin-expressing neurons, and activity in superficial layers is weaker and prolonged, facilitated by slow inhibition from GABAergic neurons expressing the 5HT3a receptor. Somatostatin-expressing GABAergic neurons do not receive direct input in either layer and their spontaneous activity is suppressed during POm stimulation. This novel pattern of weak, delayed, thalamus-evoked inhibition in layer 2 suggests a longer integration window for incoming sensory information and may facilitate stimulus detection and plasticity in superficial pyramidal neurons.

**Key words:** 5HT3a, parvalbumin, pyramidal, somatostatin, VIP

## Introduction

How does sensory neocortex convert input into output, to influence and drive activity in downstream brain areas? The algorithm by which neocortical circuits transform incoming sensory information is determined by the stereotyped connectivity and firing properties of neuronal cell types within the cortical column. Thus, defining the conserved architecture of these circuits within and between different neocortical areas has been of great interest (Lefort et al. 2009; Bock et al. 2011; Harris and Mrsic-Flogel 2013; Pi et al. 2013; Hangya et al. 2014; Vélez-Fort et al. 2014; Yuste 2015; Harris and Shepherd 2015; Jiang et al. 2015; Lee et al. 2016; Miller 2016).

Accumulating evidence indicates that there are common principles that regulate thalamic connections within the cortical column, suggesting that this transformation might have essential similarities across different primary sensory areas. For example, thalamic input to layer 4 (L4) targets both excitatory neurons as well as fast-spiking, parvalbumin-expressing (PV) inhibitory interneurons in primary visual, auditory, and somatosensory cortex but shows weak or negligible input to somatostatin-expressing (SST) neurons (Porter et al. 2001; Cruikshank et al. 2007; Schiff and Reyes 2012; Kloc and Maffei 2014; but see Hu and Agmon 2016). These principles for sensory-related thalamic input may extend to other layers (Ji et al. 2016).

In somatosensory cortex, the thalamocortical afferents from the ventro-posterior medial (VPM) nucleus in L4 have commonly been viewed as the main source of sensory input to the neocortex. However, it has become increasingly clear that another important source of cortical input comes from the posterior medial nucleus of the thalamus (POm), a higher-order

sensory nucleus with dense axonal arborizations in L1 and L5a (Koralek et al. 1988; Chmielowska et al. 1989; Cruikshank et al. 2007; Petreanu et al. 2009; Meyer et al. 2010; Wimmer et al. 2010). Neurons residing in POm have complex receptive fields, are driven by both peripheral sensory input and cortical feedback from motor and sensory areas, and are modulated by whisker movement (Diamond et al. 1992; Ahissar et al. 2001; Yu et al. 2006, 2015; Groh et al. 2014; Urbain et al. 2015). This suggests that POm, like the pulvinar in the visual system, incorporates contextual information and brain state with sensory information (Purushothaman et al. 2012; Roth et al. 2016). However, the role of higher-order thalamic nuclei in sensory processing is a topic of substantial debate (Constantinople and Bruno 2013; Yu et al. 2015; Mease et al. 2016; Roth et al. 2016; Sherman 2016), and much less is known about the distribution of POm inputs across diverse cell types, or how they drive the cortical circuit.

While prior studies have characterized the presence and sub-cellular location of POm inputs onto pyramidal (Pyr) neurons in superficial and deep layers (Bureau et al. 2006; Petreanu et al. 2009; Viaene et al. 2011; Gambino et al. 2014; Jouhanneau et al. 2014), a comprehensive analysis of inputs across multiple layers and cell types has not been accomplished. This is particularly important for developing schema by which POm can drive network activity, where inhibitory neurons can play a powerful and diverse role. Understanding the algorithm by which sensory information is transformed by neocortical circuits will be impossible without fine-grained mapping. Here we use the mouse somatosensory (barrel) cortex as a model system to define the process by which the neocortex receives and transmits incoming sensory information, with a focus on input from the higher-order thalamic nucleus POm. We perform a systematic evaluation of POm-mediated excitatory drive to barrel cortex using the experimental precision afforded by recordings in acute brain slices to target 4 defined cell types across the column.

Using channelrhodopsin (ChR2)-mediated excitation of POm fibers in the neocortex, we first determined which layers and specific cell types receive strong input. Next, we isolated layer-specific properties of disynaptic, feedforward inhibition. Finally, we investigated how these wiring motifs were manifested in recurrent activity generated by repetitive POm stimulation. Our analysis reveals thalamic wiring principles that are conserved between L4 and L5 as well as novel mechanisms for feedforward inhibition in L2. We find that direct POm input to PV cells is strong in L5a but absent in L2, where POm activity drives firing in 5HT3a-expressing (5HT3a) cells. In both layers, direct synaptic input to SST neurons was negligible. These wiring patterns generate layer-specific processing of POm thalamocortical inputs, with temporally precise spikes in L5 Pyr neurons and weak but summating responses in L2 Pyr neurons. Our results show, for the first time, that a higher-order thalamic nucleus can drive activity in multiple cell types throughout the column, and supports the idea that sensory information processing is fundamentally different across cortical layers.

Our data also recapitulate some cell-type-specific features of sensory-evoked activity—SST neuron hyperpolarization, and the initiation of recurrent network activity—that have been observed in vivo (Gentet et al. 2012; Jouhanneau et al. 2014; Mease et al. 2016), indicating that POm activity is sufficient to generate these phenomenon in acute brain slices with only local connections preserved. The ability to employ a functional readout of summated network interactions between multiple cell types with precise input control provides new insight into how large groups of interconnected neurons in the neocortex might behave during sensation.

## Materials and Methods

All experimental procedures were conducted in accordance with the NIH guidelines and were approved by the Institutional Animal Care and Use Committee at Carnegie Mellon University.

### Viral Injections and Mouse Strains

ChR2 tagged with m-cherry (300–400 nl; AAV1.CAG.hChR2 (H134R)-mCherry.WPRE.SV40, ID no. AV-1-20938 m, PENN Vector Core, Philadelphia, PA) was stereotaxically injected into the POm following a small craniotomy (bregma −1.7, lateral 1.00, depth 3.25 mm) of isoflurane-anaesthetized mice aged postnatal day 10–15 (P10-15) using a Hamilton syringe (Hamilton; Reno, NV), Stoelting infusion pump (Stoelting; Wood Dale, IL, Model #53210), and custom injection cannulas (Plastics One; Phoenix, AZ). To avoid injection spillover into VPM, injections were targeted toward the medial portion of POm. In some animals, areas of the parafasicular nucleus were labeled; however, since this nucleus does not have direct cortical projections (Allen Brain mouse connectivity atlas; http://connectivity.brain-map.org/) it is unlikely that it contributed to the responses observed in S1. After injection mice were treated once with ketoprofen (5 mg/kg, Sigma-Aldrich; St. Louis, MO) and additional doses were administered as necessary. Mice recovered in their home cage for 6–10 days prior to preparation of acute brain slices. Experiments targeting excitatory neurons were performed on C57Bl6 mice (Harlan). Specific inhibitory neuron populations were targeted using the following transgenic mice: *Sst-IRES-Cre* (Jackson Labs stock # 013044) (Taniguchi et al. 2011), *Pvalb*$^{tm1(cre)Arb}$ (Jackson Laboratory stock # 017320) (Hippenmeyer et al. 2005), *5HT3a-cre* (GENSAT 036680-University of California -Davis), and VIP-Cre (Jackson Labs stock # 010908) (Taniguchi et al. 2011), and some excitatory neurons were recorded from these lines as well. Mice were mated with Ai3 (Jackson Laboratory Stock # 007903) mice to create heterozygous transgenic mice with yellow fluorescent protein (YFP)-labeled SST, PV, 5HT3a, or vasoactive intestinal peptide (VIP) interneurons.

### Slice Preparation and Injection Site Confirmation

Injected mice were sacrificed at age P16-25 by brief isoflurane anesthesia and decapitation. Coronal slices 350 μm thick were prepared in regular ice-cold artificial cerebrospinal fluid (ACSF) composed of (in mM): 119 NaCl, 3.5 KCl, 1 $NaH_2PO_4$, 26.2 $NaHCO_3$, 11 glucose, 1.3 $MgSO_4$, and 2.5 $CaCl_2$ equilibrated with 95%/5% $O_2/CO_2$. Slices were allowed to recover at room temperature for 45 min in the dark before recording.

The injection site was confirmed anatomically using the mCherry-tagged ChR2 fluorescence in cell bodies at the injection site and the characteristic pattern of fluorescent axonal labeling in the barrel cortex, concentrated in L1 and L5a (Wimmer et al. 2010). Only slices that had fluorescently labeled axons in both L1 and L5 but not in L4 were used in our experiments. Retrogradely labeled, ChR2$^+$ neurons in the somatosensory cortex were never observed.

### General Electrophysiology

In slices with confirmed injections, cortical excitatory Pyr neurons and identified inhibitory neurons were targeted for whole-cell recording in the posteromedial barrel subfield using an

Olympus light microscope (BX51WI) with a mercury lamp for fluorescence imaging and borosilicate glass electrodes resistance 4–8 MΩ. Electrode internal solution, except for a small subset of experiments described later, was composed of (in mM): 125 potassium gluconate, 10 HEPES, 2 KCl, 0.5 EGTA, 4 Mg-ATP, and 0.3 Na-GTP, pH 7.25–7.30, 280 mOsm. For some cells trace amounts of AlexaFluor 594 were added to the internal solution to confirm cell targeting. Electrophysiological data were acquired using a Multiclamp 700B amplifier (Axon Instruments, Foster City, CA) and a National Instruments acquisition interface (National Instruments; Austin, TX). The data were filtered at 3 kHz, digitized at 10 kHz, and collected using custom macros in Igor Pro 6.0 (Wavemetrics, Lake Oswego, OR).

## Cell Identification

The morphology and basic electrophysiological properties of all recorded cells were evaluated to aid in cell identification: resting membrane potential ($V_{Rest}$), input resistance ($R_i$), series resistance ($R_s$), and firing phenotype using brief depolarizing currents in current clamp (see Supplementary Tables 1 and 2). Cells were allowed to equilibrate for 5 min before data collection. Following recording, cells were imaged to determine neurite morphology if fluorescently filled and to measure their laminar location based on depth from pial surface and relevant cytoarchitectural features. L2 neurons were defined as neurons up to 100 um below the cell-sparse area of L1, typically 50–150 um below the pial surface. L3 neurons were selected 100 um above the L4 barrel, visually identifiable under bright field illumination. These criterion necessarily excluded cells at the margin of L2 and L3, since they could not be unambiguously assigned. L4 neurons are defined as inside the upper and lower limit of the L4 barrel, but were selected from both "barrel" and "septal" regions, since segregated barrel and septal circuits in mouse L4 are absent (Feldmeyer et al. 2013). L5a neurons made up the visually identifiable area ~150–200 um below the L4 barrels corresponding to the location of fluorescent POm axons. L5b was defined as the area up to 150 um below L5a, and L6 was defined as the 150 um above the white matter. Cre-dependent YFP fluorescence within a cell population reflected well-defined electrophysiological properties and firing phenotype (Agmon and Connors 1992; Kawaguchi and Kubota 1997; Lee et al. 2010; Xu et al. 2013; Neske et al. 2015). SST cells had a medium to large input resistance (536 ± 71 MΩ) with a low-threshold-spiking firing phenotype that showed rate and amplitude accommodation. A small number of SST cells identified by reporter expression exhibited a FS firing phenotype (Tan et al. 2008) and were excluded from further analysis. Notably, their POm responses obeyed their firing phenotype classification rather than their SST marker gene expression. PV neurons had a very low $R_i$ (286 ± 34 MΩ) and a fast-spiking firing phenotype. 5HT3a cells, which are known to be a heterogeneous population, displayed diverse electrophysiology properties and firing phenotypes (Lee et al. 2010). Excitatory neurons were characterized by a Pyr soma morphology, a regular spiking firing phenotype, intermediate $R_i$ (354 ± 23 MΩ), and presence of dendritic spines when fills were available. $R_s$ and $R_i$ were monitored for the duration of experiments and cells with $R_i$ below 100 MΩ, $R_s$ > 45 MΩ, or where $R_s$ changed by more than 30% over the course of data collection were excluded from further analysis.

## POm Synaptic Input

To assess excitatory synaptic input to cell populations, POm axons were stimulated optically while holding cells at −70 mV, the calculated $E_{Cl}$. Single or paired 5 ms light pulses (12.5 Hz, 479 nm) were delivered through a 40× water-immersion objective (Olympus) at the recording site using a white LED (Prizmatix; Israel) in combination with an 40 nm excitation filter centered at 480 nm (Chroma; Bellows Falls, VT). Light intensity at 470 nm was measured at 2.13 mW, distributed over a beam area ~1 mm diameter, in line with parameters employed in similar slice experiments (Petreanu et al. 2007; Cruikshank et al. 2010; Kinnischtzke et al. 2014). Timing of optogenetic simulation was controlled by a Master-8 (A.M.P.I; Jerusalem, Israel). All experiments were performed at a maximum light intensity to allow for better comparison of currents and timing across experiments. Stimulus trials were carried out at low frequency (0.05 Hz). For all cells and conditions, responses following stimulation were averaged across 10 trials and the amplitude of POm-evoked excitatory post-synaptic current (EPSC) was taken as the peak amplitude in the 50 ms following stimulus onset for events with an onset latency of <10 ms post-stimulus. Responses below 3 pA could not be resolved from noise and were given a value of 0. Paired-pulse ratio for POm-evoked responses was calculated by measuring EPSC amplitude for 2 responses at an 80 ms interstimulus interval. To confirm that the observed input was glutamatergic, the AMPA receptor antagonist NBQX (10 μM, Sigma-Aldrich; St. Louis, MO) was applied in a subset of experiments.

To isolate direct POm-evoked responses in excitatory and inhibitory neurons, the voltage-gated sodium channel antagonist tetrodotoxin (TTX) (0.25–0.5 μM, Sigma-Aldrich; St. Louis, MO) was applied to prevent polysynaptic activity along with 100 μM 4-aminopyridine (4-AP) (Sigma-Aldrich; St. Louis, MO) to assist in axonal depolarization and neurotransmitter release (Petreanu et al. 2009). As a positive control, a light-triggered POm response had to be recorded in a Pyr neuron in each slice for each condition to be included in analysis to insure that the absence of a light-evoked response was not caused by low levels of viral transduction.

## Laminar Input to Excitatory and Inhibitory Neurons

The amplitude of direct POm input was recorded in TTX and 4-AP for excitatory Pyr neurons across multiple cortical layers within a single slice; at least 1 L5a Pyr neuron was recorded from in every slice.

POm input onto SST, PV, and 5HT3a neuron populations were recorded in separate experiments using different transgenic mice. In a subset of animals, immunohistochemistry was performed against YFP to visualize the distribution of each inhibitory neuron population across cortical layer. In each slice, interneurons and Pyr neurons (<200 μm apart) were recorded in pairs or sequentially to account for across-animal differences in viral expression. POm-evoked EPSCs in inhibitory neurons, and their corresponding Pyr neurons, were recorded as described above in ACSF and in the presence of TTX and 4AP to reveal all input and direct input respectively. For a subset of L2 and L5 SST neurons we delivered long stimulus trains (10+ pulses, 80 ms ISI) to identify any facilitating responses with and without TTX and 4-AP.

## Polysynaptic Inhibition and AP Generation

In a subset of experiments we characterized POm-evoked polysynaptic inhibition onto L2 and L5a excitatory neurons by recording in current clamp. Here, the EPSP and IPSP amplitude was calculated as the maximum depolarization or hyperpolarization following POm-stim.

For isolating inhibitory post-synaptic current (IPSC) in voltage clamp, L2 and L5a Pyr neurons were held at +10 mV using a Cs-based internal solution containing (in mM): 130 cesium gluconate, 10 HEPES, 0.5 EGTA, 8 NaCl, 10 Tetraethylammonium chloride (TEA-Cl), 4 Mg-ATP and 0.4 Na-GTP, pH 7.25–7.30, 280–290 mOsm. POm-evoked EPSCs and IPSCs following 5 ms optogenetic stimulation of POm fibers (same as above) were averaged across 10 trials and the magnitude was taken as the maximum amplitude within 50 ms following stimulus onset. Rise and decay times for each cell were measured from the cell average IPSC (10 sweeps). Rise time was measured from 10% to 90% and decay time was measured as the time from response peak to return to 1/3 of the max amplitude. Decay time and inhibitory to excitatory current ratio was calculated for both maximum stimulation and a minimal stimulation where light intensity was decreased until single, smooth IPSCs were elicited.

To determine which inhibitory neuron populations mediate the polysynaptic inhibition observed in L2 and L5a Pyr neurons, AP generation and timing was assessed for all cell types in ACSF. Cell responses to a single 5 ms light pulse were recorded in current clump at resting membrane potential for each neuron. Cells that fired APs on any of 5 consecutive sweeps were designated as firing APs. For each cell, the average spike time was determined by taking the mean average of the spike peak latency following stimulus onset for 5 consecutive sweeps. The amplitude of POm-evoked EPSPs and IPSPs was also recorded for each cell population, but could not be calculated for neurons that fired APs on every trial.

### Ongoing POm Stimulation and Recurrent Activity

To determine the effect of ongoing POm activity on cortical network dynamics we delivered trains of light pulses while recording in a modified ACSF solution (mACSF, in mM: 119 NaCl, 2.5 KCl, 1 $NaH_2PO_4$, 26.2 $NaHCO_3$, 11 glucose, 0.5 $MgSO_4$, and 1 $CaCl_2$) which simulates the neuronal activity levels observed in vivo (Urban-Ciecko et al. 2015) and allows for recurrent network activity. We recorded from L2 and L5 Pyr, SST, PV, 5HT3a, and VIP neurons in current clamp while delivering trains of 5 ms light pulses at 12.5 Hz at an inter-trial interval of 0.05 Hz. This frequency is physiologically relevant and matches the firing rates observed for POm cells in awake, behaving animals (Urbain et al. 2015). For each cell, 10 consecutive trials were recorded and displayed as overlays of all trials and as a raster plots that show AP peak time for each trial. Spike data was binned at 40 ms intervals and averaged across all cells of a given population to generate an average post-stimulus time histogram. Some cells displayed prolonged epochs of depolarization and AP generation similar to an upstate following POm activation, and were included in analysis. In vivo, SST cells rest depolarized and fire spontaneously (Gentet et al. 2012) so SST cells when necessary were given a depolarizing holding current to adjust $V_m$ to –48 mV ± 2 mV, allowing us to measure POm-evoked hyperpolarization and modulation of firing frequency.

For each cell type, the average firing rate was calculated for 500 ms pre-stim (i.e. spontaneous activity), during stim, and post-stim, displayed in Supplementary Table 2. In SST neurons, the length of hyperpolarization was different across cells therefore the during-stimulus bin is calculated for 40–160 ms post-stim to capture the consistent early hyperpolarization observed.

### Statistical Analysis

For each analysis as described throughout, values were measured from average responses of 10 consecutive sweeps unless otherwise noted. Unless indicated, calculations and statistics were performed on cells and all statistical tests are non-parametric Wilcoxon rank sum tests. Standard error of the mean is reported with all averages and as error bars unless otherwise reported. Cell (*n*) and animal values (*N*) are reported in each figure.

## Results

### POm Provides Direct, Glutamatergic Input Onto Cortical Excitatory Neurons

To understand how POm activity is transformed by somatosensory cortex, we first mapped this input onto excitatory neurons across the cortical column. Prior studies have suggested that POm stimulation both in vivo and in vitro can drive short latency, excitatory responses in some neocortical neurons (Bureau et al. 2006; Petreanu et al. 2009; Viaene et al. 2011; Gambino et al. 2014; Jouhanneau et al. 2014), but how they are distributed across excitatory neurons throughout the cortical column and within different cell types in a given layer has not been comprehensively investigated. To determine how POm inputs engage excitatory neurons from L2 to L6, we used a ChR2-based strategy to selectively excite POm afferents in combination with pharmacological methods to evaluate whether these inputs directly activated target neurons.

POm-targeted stereotaxic injections of ChR2-expressing virus were carried out in young postnatal mice, and POm targeting in acute brain slices was confirmed by a characteristic pattern of afferent labeling concentrated in L5a and L1 of S1 barrel cortex (Koralek et al. 1988, Meyer et al. 2010). In cases where the injection site overlapped slightly with the VPM nucleus of the thalamus, we could observe terminal labeling both in L4 (the VPM target layer) and L5a/L1, and this tissue was not used for further analysis.

Broad-field illumination of ChR2 afferents with a 5 ms blue light pulse elicited a short latency EPSC in Pyr neurons (Fig. 1). These responses were eliminated in the presence of the AMPAR antagonist NBQX, indicating that POm input was glutamatergic (Fig. 1*B*). For both L2 and L5 neurons, paired-pulse optical stimulation showed that responses were depressing (see Supplementary Table 1), likely due to elevated initial release probability from ChR2-mediated depolarization.

To confirm that this excitation results from direct input from POm and not recurrent activation elsewhere in the neocortical circuit, TTX and 4-AP were bath applied to prevent network firing (Petreanu et al. 2009). Here, $Ca^{++}$-dependent synaptic release is thought to be mediated by ChR2-depolarization at the terminal that directly enables opening of voltage-gated $Ca^{++}$ channels, and the addition of the $K^+$ channel blocker 4-AP increases the period of depolarization at the terminal to enhance release. In all cases, the EPSC persisted, although the onset latency and time to EPSC peak was increased slightly, most likely due to prolonged depolarization at the terminal (Fig. 1*C*).

To systematically compare ChR2-mediated POm input strength across the entire column, excitatory neurons in each layer were targeted for voltage-clamp recordings. POm fiber activation generated the largest amplitude responses in L5a neurons (Fig. 1*D–F*), consistent with the large density of fibers in this layer, and mean evoked EPSC amplitude for L5a neurons was nearly 5-fold greater in these neurons than for any other excitatory neurons in other layers (Fig. 1*F*). To more accurately compare input strength across different preparations with varying levels of ChR2 expression, responses across the column

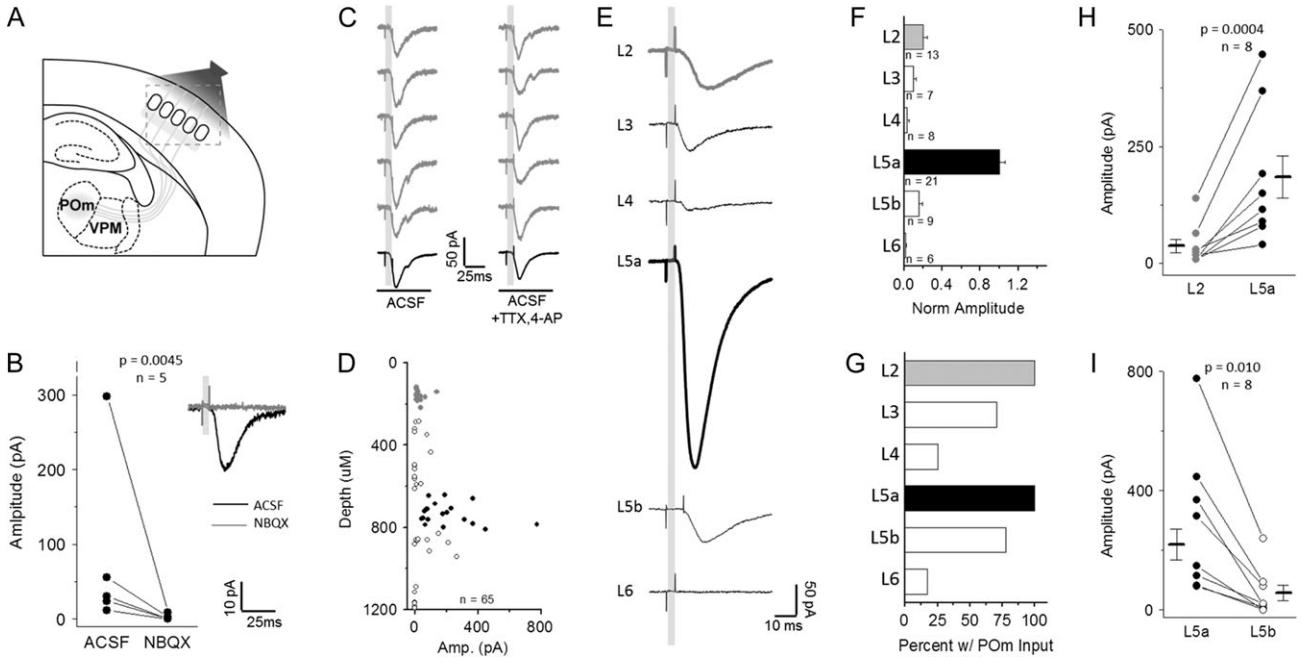


**Figure 1.** Excitatory neurons in all cortical layers receive direct synaptic input from POm. (*A*) Schematic of experimental design. POm-targeted ChR2 viral injection in POm neurons labeled axons in barrel cortex. (*B*) EPSCs evoked by POm light stim in L2 Pyr neurons, eliminated by addition of AMPAR antagonist NBQX. About 5 consecutive trials (gray) followed by response average for 10 trials. (*C*) Short latency EPSCs in L2 Pyr neurons are direct from POm axons. EPSCs persist with addition of voltage-gated $Na^+$ channel antagonist TTX and K-channel antagonist 4-AP. (*D*) Direct POm-evoked EPSCs in cortical Pyr neurons in TTX and 4-AP plotted by depth from pia surface (gray: L2, black: L5a). (*E*) Average cell response (10 trials) for a representative cell in each cortical layer, defined by cytoarchitecture and depth. (*F*) Across-layer comparison of amplitude normalized to the average L5a response in each slice to account for across-preparation variance in ChR2 expression. (*G*) Percent of recorded cells in each layer that receive direct POm-evoked EPSCs. (*H*) L5a Pyr neurons receive larger direct input than in L2. Connected points represent a comparison of the average of all responses recorded in L2 or L5a neurons from a given animal. Data points and *n* value are animal averages and a paired *t*-test is used. (*I*) L5a Pyr neurons receive larger direct POm input than L5b neurons; same as (*H*).

were normalized to the mean strength of POm input to L5a neurons recorded in the same brain slice. Within the same slice, mean EPSC amplitude was always larger in L5a than L2 neurons (Fig. 1*E*,*F*,*H*); a difference that was highly significant. Recordings from neurons whose cell bodies resided in L5b showed significantly weaker POm input, although >75% of these cells received some direct input (Fig. 1*G*,*I*).

Although previous studies suggested POm inputs might be unevenly distributed across neurons in L2 and L5 (Bureau et al. 2006; Viaene et al. 2011), our method revealed that 100% of L2 and L5a neurons received some POm input (Fig. 1*G*). Relative input strengths for Pyr neurons in L2 and L5 are also generally consistent with prior studies using optogenetic activation, although we observed substantially larger relative excitation for L5b Pyr neurons compared to other reports (Petreanu et al. 2009). Notably, at least a subset of excitatory neurons in all layers received synaptic POm input, although this input was more sparsely distributed and weakest in amplitude in L4 and L6, major targets for VPM afferents (Wimmer et al. 2010). Overall, we find that neurons whose cell bodies reside in L2 and L5 are the primary targets for POm-mediated sensory input, with the strongest input found in L5a. These findings are consistent with the distribution of POm fibers in the cortical column (Meyer et al. 2010) and suggest that POm-mediated information transfer to the neocortex will be initiated by circuit activity in these layers.

## GABAergic Neuron Subtypes Differentially Receive Direct POm Input in L5

Cortical transformations of thalamic input will depend on the activity of both excitatory and inhibitory neurons. To identify principles of thalamic connectivity to specific subtypes of inhibitory neurons, we took advantage of 3 different Cre driver lines of transgenic mice to identify the major subset of inhibitory neurons; SST-, PV-, and 5HT3a-expressing cells (Fig. 2*B*–*D*) (Hippenmeyer et al. 2005; Gong et al. 2007; Taniguchi et al. 2011). Together, these subtypes of inhibitory cells account for nearly 100% of all cortical GABAergic neurons (Rudy et al. 2011).

VPM thalamic input to L4 interneurons has been shown to mainly target PV cells (Cruikshank et al. 2007, but see Porter et al. 2001; Hu et al. 2016). To test whether this pattern of innervation was input- (both POm and VPM) and layer- (both L5 and L4) specific, PV neurons were genetically labeled using a PV-Cre driver line crossed to the Ai3 YFP reporter line, and double-transgenic mice were stereotaxically injected with ChR2 virus in POm.

PV cells in major POm recipient layers, L2 and L5, were targeted for whole-cell voltage-clamp recordings (Fig. 2*B*,*E*,*F*). In all experiments, Pyr cell responses were obtained in each slice to directly compared input strength between these cells and adjacent inhibitory neurons. Under conventional recording conditions (ACSF), POm-driven EPSCs were detected in all PV cells and the mean amplitude of this response was similar between PV and Pyr cells (Fig. 2*E*,*K*; 7/7 PV cells responding; all cell mean PV −269 ± 48 vs. Pyr −325 ± 44 pA). These responses persisted in the presence of TTX and 4-AP (Fig. 2*F*,*L*; 6/6 PV cells responding; all cell mean PV −87.6 ± 24 vs. Pyr −45.9 ± 8.2 pA), indicating that they result from direct synaptic input from POm afferents to PV cells.

In contrast to strong input to PV neurons, light-evoked POm activation yielded no or a barely detectable EPSC in SST neurons, despite a robust response in adjacent L5 Pyr cells (Fig. 2*C*,*E*,*K*;

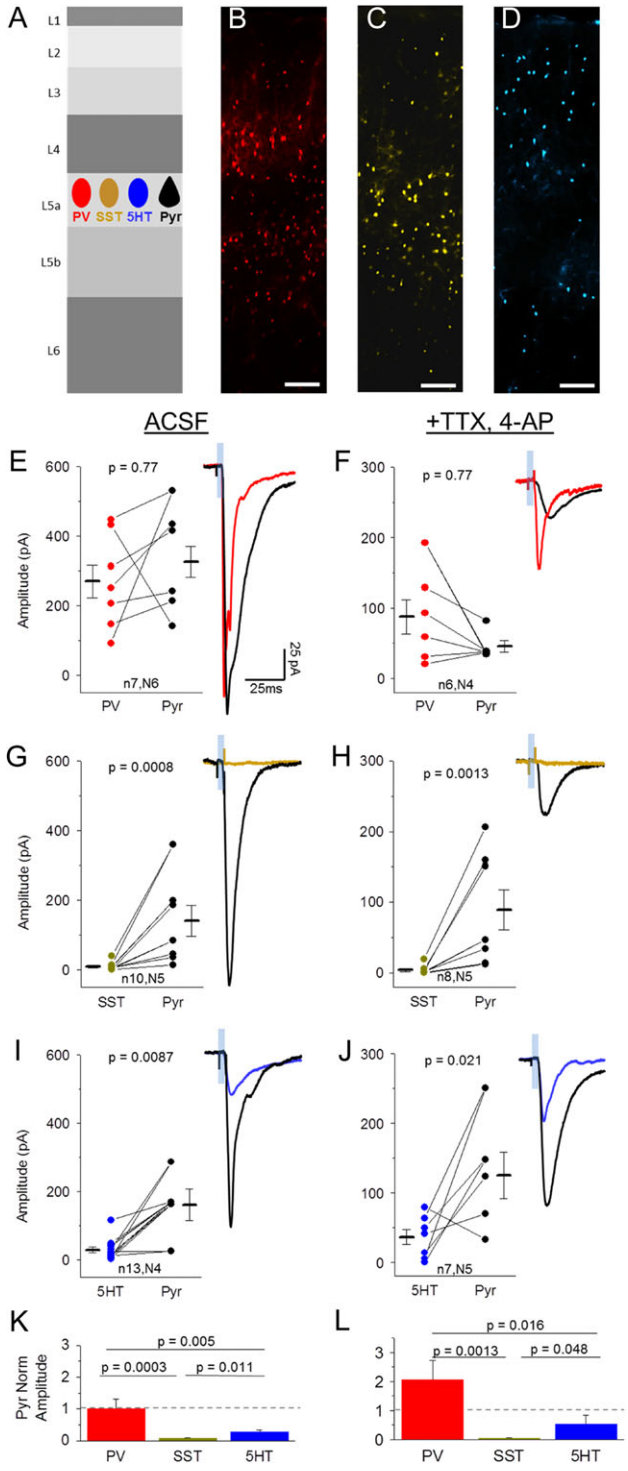


**Figure 2.** Direct synaptic inputs from POm onto 3 major interneuron classes in L5. (*A*) Schematic of experiment. Light-evoked EPSCs were recorded in labeled inhibitory neurons (PV-, SST-, 5HT3a-Cre X Ai3) and Pyr neurons in L5 of POm-ChR2 injected animals. (*B–D*) Laminar location of fluorescent PV (*B*), SST (*C*), and 5HT3a (*D*, abbreviated 5HT for brevity) inhibitory neurons, scale bar: 100 uM. (*E,F*) Comparison of peak (within 50 ms of stim onset) POm-evoked EPSC amplitude (average, 10 trials) of a PV cell and nearby Pyr neuron (<300 um apart) in ACSF (*E*) and TTX, 4-AP (*F*). Sample trace shows PV (red) and Pyr (black) average response to 5 ms light pulse in same slice. (*G,H*) POm-evoked responses of SST (yellow) and nearby Pyr (black) neurons in ACSF (*G*) and TTX, 4-AP (*H*). (*I,J*) POm-evoked responses of 5HT (blue) and nearby Pyr (black) neurons in ACSF (*I*) and TTX, 4-AP (*J*). (*K,L*) Average of inhibitory neuron response amplitudes normalized to nearby Pyr neurons in rACSF (*K*, analysis of variance [ANOVA] *P*-value: 0.0017) and TTX, 4-AP (*L*, ANOVA *P*-value: 0.011). *N* values correspond to values in *E–J*. Note that inhibitory neurons are compared to multiple Pyr neurons when more than 1 Pyr neuron was recorded in the same slice.

6/10 SST responding; all cell mean, SST −8.3 ± 4 vs. Pyr −140 ± 45 pA). Across different lines of transgenic mice, we found that the mean amplitude of SST responses was 30-fold lower than observed for PV cells in L5.

To determine whether these small responses resulted from direct thalamic input, POm stimulation was carried out with TTX and 4-AP in the bath. Under these conditions, short latency EPSCs were virtually eliminated (Fig. 2*H,L*; 2/8 cells SST responding; all cell mean SST −4.1 ± 2 vs. Pyr −89.2 ± 28 pA). These data indicate that, like in L4 (Cruikshank et al., 2007; but see Tan et al., 2008; Hu and Agmon 2016), thalamic input to L5 SST neurons is negligible to non-existent, and suggest that this might be a conserved wiring principle across layers.

Although PV and SST neurons make up >90% of the inhibitory neuron population in L5, 5HT3a-expressing cells are sparsely present (Fig. 2*D*) (Lee et al. 2010; Rudy et al. 2011). POm-driven EPSC amplitudes in this population were on average larger than those observed in SST neurons but still 10-fold lower than adjacent L5a Pyr neurons (Fig. 2*I,K*; 8/9 5HT3a cells responding; all cell mean, 5HT3a −33.9 ± 11 vs. Pyr −166 ± 2.0 pA). Input strength was heterogeneous in these cells, consistent with the diversity of cell types within this population (Staiger et al. 1996; Lee et al. 2010; Miyoshi et al. 2010).

POm-driven EPSCs onto 5HT3a-expressing neurons remained in the presence of TTX and 4-AP (Fig. 2*J,L*; 4/5 5HT3a cells responding; all cell mean, 5HT3a −31.9 ± 11 vs. Pyr −156 ± 43 pA), indicating that this sparse cell population in L5 receives small but direct input from the thalamus. This connectivity motif has previously been observed for VPM inputs onto 5HT3a neurons in L4 (Staiger et al. 1996; Lee et al. 2010). POm input was significantly greater for PV cells compared to SST and 5HT3a neurons (Fig. 2*K,L*).

Overall, the principles of thalamic connectivity to L5 appear similar to those described for VPM inputs to L4, with strong drive to PV neurons, weak and heterogeneous input to 5HT3a neurons (Ji et al. 2016), and virtually non-existent input to low-threshold spiking SST neurons (Staiger et al. 1996; Porter et al. 2001; Swadlow and Gusev 2002; Cruikshank et al. 2007; Tan et al. 2008; Lee et al. 2010; Chen et al. 2015; Hu and Agmon 2016). Strong thalamic drive to PV neurons is observed for thalamocortical inputs to L4 in other primary sensory areas as well, suggesting that this may be a conserved motif for thalamocortical inputs throughout the brain (Schiff and Reyes 2012; Kloc and Maffei 2014; Delevich et al. 2015; Ji et al. 2016).

## Thalamic Input is Differentially Distributed Across L2 Inhibitory Populations

To determine whether these principles of thalamic input were conserved for POm inputs in superficial layers, we investigated cell-type-specific POm responses in the 3 broad classes of inhibitory neurons described above.

Surprisingly, PV cells in L2 showed negligible responses to POm afferent stimulation. Mean POm-evoked EPSC amplitude in L2 PV cells was nearly 10-fold lower (3/6 responding, all cell mean −4.8 ± 1 pA) than what was observed in adjacent Pyr neurons (−43.5 ± 7.6 pA), a difference that was highly significant (Fig. 3*B,H*). This small response was eliminated in TTX and 4-AP (Fig. 3*C,I*; 1/8 PV cells responding; all cell mean, PV −0.9 ± 0.5 vs. Pyr −24.0 ± 5.4 pA). The lack of direct thalamic input to fast-spiking PV neurons suggested that neocortical transformations in this layer might be mediated through different principles than observed in deeper layers, either through a different population of interneurons or through reduced overall inhibition.

Targeted voltage-clamp recordings of SST neurons in L2 showed that, like L5, these cells receive little to no POm input

compared to adjacent Pyr neurons (Fig. 3*D*,*H*; 3/9 SST cells responding, all cell mean −3.22 ± 1.3 vs. Pyr −47.6 ± 11 pA). Indeed, in the presence of TTX and 4-AP, responses were eliminated (Fig. 3*E*,*I*; 0/9 SST cells responding; all cell mean SST −0.77 ± 0.3 vs. Pyr −30.3 ± 10 pA).

Because excitatory inputs to SST neurons are strongly facilitating (Silberberg and Markram 2007; Fanselow et al. 2008; Urban-Ciecko et al. 2015), we considered the possibility that release probability might be too low to detect a response after a single POm stimulus. To determine whether weak POm input might be revealed with repetitive POm stimulation as has been suggested in L4 (Tan et al. 2008; Hu and Agmon 2016), a train of 10+ light pulses was delivered during SST-recordings in both L2 and L5 (see Supplementary Fig. S1). In many cases POm drove a small, direct EPSC in an SST neuron (ACSF 4/5 cells; TTX, 4AP ¾ cells); notably, these responses were depressing, suggesting that ChR2-mediated release is highly efficient. In other SST cells (ACSF 1/5 cells; TTX 4AP ¼ cells), no synaptic response was observed even after a 10-pulse train (12.5 Hz), indicating that these neurons do not receive weak and facilitating inputs from the higher-order thalamic nucleus POm (Tan et al. 2008; Hu and Agmon 2016).

5HT3a-expressing cells are abundant in L1 and 2 and account for half of all GABAergic neurons in superficial layers (Fig. 2*D*) (Rudy et al. 2011). Whole-cell current clamp recordings confirmed that these cells are heterogeneous, composed of irregular spiking, late-spiking, fast-adapting, and other cell types (Lee et al. 2010). Because 5HT3a cells do not show a clear distinction between L1 or L2—and are frequently clustered at the border of these 2 layers making layer assignment difficult—these cells were grouped for further analysis.

Targeted recordings of 5HT3a-labeled cells showed that these neurons as a group are significantly more likely to receive POm input compared to SST or PV cells (13/16 cells), although

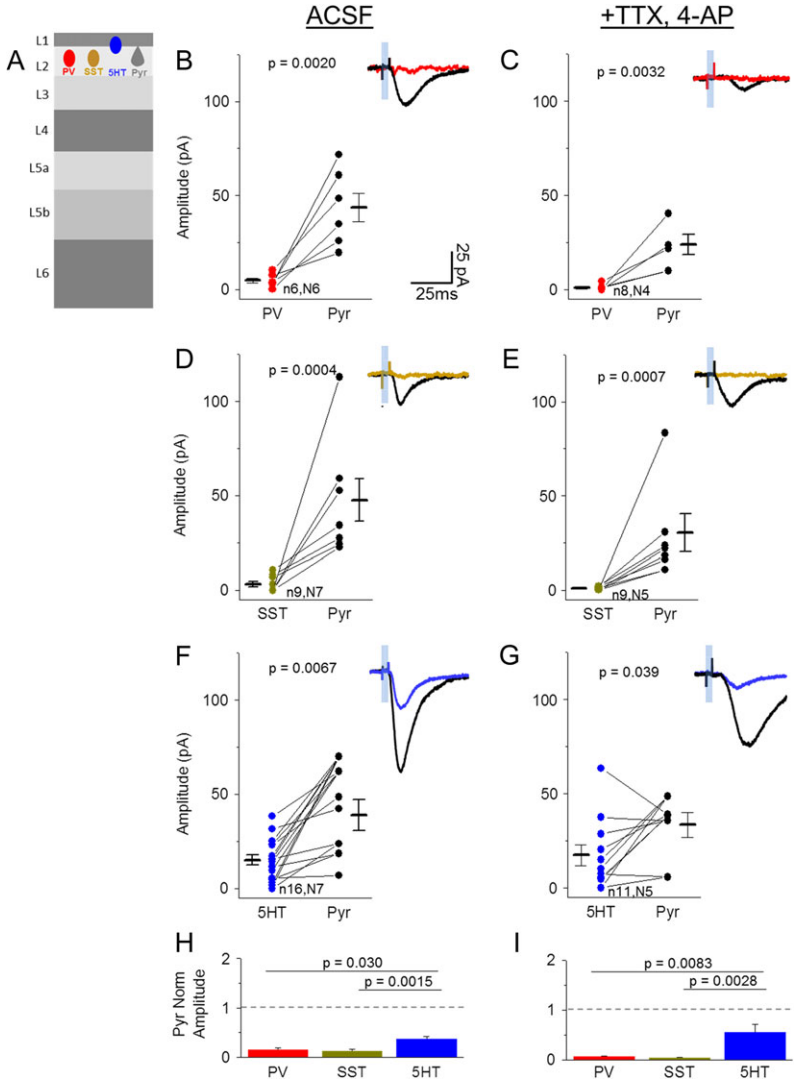


**Figure 3.** Direct synaptic input from POm onto 3 major interneuron classes in L2. (*A*) Schematic of experiment. Light-evoked EPSCs were recorded in labeled inhibitory neurons (PV-, SST-, 5HT-Cre X Ai3) and Pyr neurons in L2 of POm-ChR2 injected animals. (*B*,*C*) Comparison of peak (within 50 ms stim onset) POm-evoked EPSC amplitude (average, 10 trials) of a PV cell and nearby Pyr neuron (<300 um apart) in control ACSF (*B*) and TTX, 4-AP (*C*). Sample trace shows PV (red) and Pyr (black) average response to 5 ms light pulse in same slice. (*D*,*E*) POm-evoked responses of SST (yellow) and nearby Pyr (black) neurons in ACSF (*D*) and TTX, 4-AP (*E*). (*F*,*G*) POm-evoked responses of 5HT (blue) and nearby Pyr (black) neurons in ACSF (*F*) and TTX, 4-AP (*G*). (*H*,*I*) Average of inhibitory neuron response amplitude normalized to nearby Pyr neurons in rACSF (*H*, ANOVA *P*-value: 0.0053) and TTX, 4-AP (*I*, ANOVA *P*-value: 0.0049). *N* values correspond to values in *B*–*G*. Note that inhibitory neurons are compared to multiple Pyr neurons when more than 1 Pyr neuron was recorded in the same slice.

input strength was heterogeneous across the group (Fig. 3F–I). POm-evoked EPSC amplitudes appeared greater in adjacent Pyr cells (all cell mean 5HT3a −15.1 ± 2.7 vs. Pyr −38.9 ± 8.2 pA). Responses were maintained in TTX and 4-AP, indicating that most 5HT3a neurons receive direct POm input (Fig. 3G,I; 9/11 5HT3a cells responding; all cell mean −17.5 ± 5.6 vs. Pyr −33.4 ± 6.5 pA), similar to inputs from primary thalamic nuclei in granular layers (Staiger et al. 1996; Lee et al. 2010; Wall et al. 2016; but see Ji et al. 2016).

Overall, these results predict that thalamocortical transformations in deep and superficial layers may be fundamentally different, where feedforward inhibition from PV cells in L5 may shape the flow of excitation in this layer but 5HT3a neurons assume this role in superficial layers.

## POm-Driven Disynaptic Inhibition Differs Between L2 and L5a Pyr Neurons

Cell-type-specific patterns of synaptic connectivity suggest characteristic sequences of neuronal activation induced by sensory input and constrain models of how thalamic information is transformed in the neocortex. Under our recording conditions, we found that POm stimulation elicited both excitatory and delayed inhibitory synaptic responses in Pyr cells (Fig. 4 and Supplementary Fig. S2C,D). Since POm input was exclusively excitatory (Fig. 1B), we reasoned that this inhibition might be a property of the local circuit. In addition, we predicted that the pattern of direct input identified across different populations of interneurons described in Figures 2 and 3 might help identify the cellular source(s) of this inhibition.

To investigate the properties of POm-driven inhibition in L2 and L5a, we carried out voltage-clamp recordings of Pyr cells at holding potentials designed to isolate excitatory (−70 mV) and inhibitory responses (+10 mV; Fig. 4). Under conventional recordings conditions, mean EPSC onset was slightly faster in L5a than in L2 (Fig. 4C,G). Within a given cell, IPSC latency was longer than observed for EPSCs in both layers (Fig. 4B–G), consistent with disynaptic inhibition from an intermediate cortical inhibitory neuron.

Mean IPSC onset for L5a Pyr neurons was fast and regular across preparations, typically occurring <8 ms after light pulse initiation and approximately 3 ms after the EPSC onset (Fig. 4F, G; range 5.7–12.2 ms). The very short latency between the POm-driven EPSC and the IPSC was consistent with only a single synapse between these events; i.e. that it did not result from recurrent excitation or feedback inhibition.

In L2 Pyr neurons, IPSC onset occurred at a significantly longer mean latency in aggregate, at 12.6 ms ($P < 0.00001$), and the range of this latency across cells was greater than observed in L5a (Fig. 4B,C; range 8.2–18.7 ms). Interestingly, this variable latency was also observed in consecutive sweeps within a single Pyr cell in L2, where onset latency could range as much as 4.5 ms, compared with only 1.5 ms for L5a. Because the latency of interneuron firing is influenced by the level of ChR2 expression across different preparations, it was useful to directly compare IPSC onset timing for cells within the same slice. Even when compared for cells collected from the same animal, IPSC onset latency was nearly 5 ms longer in L2 than in L5a Pyr neurons (L2 11.7 ± 0.7 ms vs. L5a 7.1 ± 0.3 ms; $P < 0.0001$), indicating that inhibition in the 2 layers may originate from different sources.

Peak POm-evoked IPSC amplitudes were, on average, larger in L5 than L2 (Fig. 4; L2 380 ± 57 pA vs. L5a 927 ± 110 pA). Because L2 also showed a smaller amplitude of POm-mediated excitation, it was possible that the difference in IPSC amplitude might simply scale to overall input strength in this layer (Xue et al. 2014). However, calculating the ratio of excitation to inhibition from measured E- and IPSCs showed that inhibition was comparatively larger in L5a ($P = 0.022$, Supplementary Fig. S2G). Thus, reduced and delayed inhibition in L2 is not a direct consequence of lower overall POm drive in this layer.

POm-evoked inhibition observed in L2 and L5a also had markedly different activation kinetics and duration, suggesting different sources of inhibition onto these 2 types of neurons. IPSCs in L5 showed a fast rise and decay time (Fig. 4J,K–M), and inspection of individual evoked IPSCs indicated that the IPSC rise was smooth (Fig. 4J), suggesting synchronized inhibition. In contrast, IPSCs in L2 Pyr neurons had a slower rise and a significantly longer decay (Fig. 4I,K–M), suggesting that they might arise from a different cellular source with less synchronized activation. To determine whether the difference in decay might result from the smoothed average of delayed IPSCs in the post-stimulus window, we reduced the intensity of the light stimulus to improve IPSC isolation. Even under these conditions, the difference in duration of inhibition between L2 and L5a Pyr neurons persisted (see Supplementary Fig. S2H). Thus, POm activity drives both quantitatively and qualitatively different types of inhibition in deep versus superficial layers.

## PV Neurons Provide Fast Disynaptic Inhibition to L5a Pyr Neurons

We first investigated the cellular source of disynaptic inhibition in L5a, since this layer received the strongest overall input. Our initial experiments indicated that fast feedforward inhibition likely originates in local PV- or 5HT3a-expressing interneurons in L5, since SST neurons did not receive direct synaptic input. The low input resistance of PV neurons (see Supplementary Table 1) likely increases the amount of current required to drive spiking in these cells. However, current-clamp recordings from PV-Cre neurons revealed that under our recording conditions, ChR2-mediated activation of POm afferents was sufficient to drive reliable, short-latency firing in this population (Fig. 5D,F; 7/8 cells). Although ChR2 expression levels could differ from animal to animal, mean spike times in L5 PV cells were remarkably consistent between preparations (latency from light pulse onset 6.60 ± 0.22 ms; n = 7). Thus, PV neurons are strongly driven by POm input. Furthermore, these spikes were well-aligned to the mean IPSC onset recorded in Pyr neurons (Fig. 5D,F; 7.25 ± 0.3 ms; $n = 18$), suggesting that these cells were the source of fast, disynaptic inhibition onto L5a Pyr neurons.

In contrast, mean POm-evoked spike times in L5 5HT3a-expressing neurons were significantly delayed compared to evoked spikes observed in PV cells (Fig. 5D,F; 26.1 ± 7 ms; $n$=2/7 cells spiking; $P < 0.001$). Under our recording conditions, 5HT3a cells in L5 exhibited at most, a single spike within 80 ms of the light pulse onset (45% failure rate across trials for spiking neurons), and these spike times could vary substantially between trials even for the same neuron (Fig. 5F). 5HT3a cells that did not fire an AP still experienced a strong membrane potential depolarization on average (Fig. 5E; 8.13 ± 1.5 mV). Although both PV cells and subsets of 5HT3a neurons are synaptically connected to neighboring Pyr neurons (Pfeffer et al. 2013; Jiang et al. 2015), the close apposition of the PV spike with the onset of the IPSC in L5a Pyr cells suggests that local PV cells are the source of fast feedforward inhibition during POm-evoked activation. In addition, the fast rise and decay kinetics of disynaptic IPSCs typically recorded in Pyr cells (Fig. 4L,M)

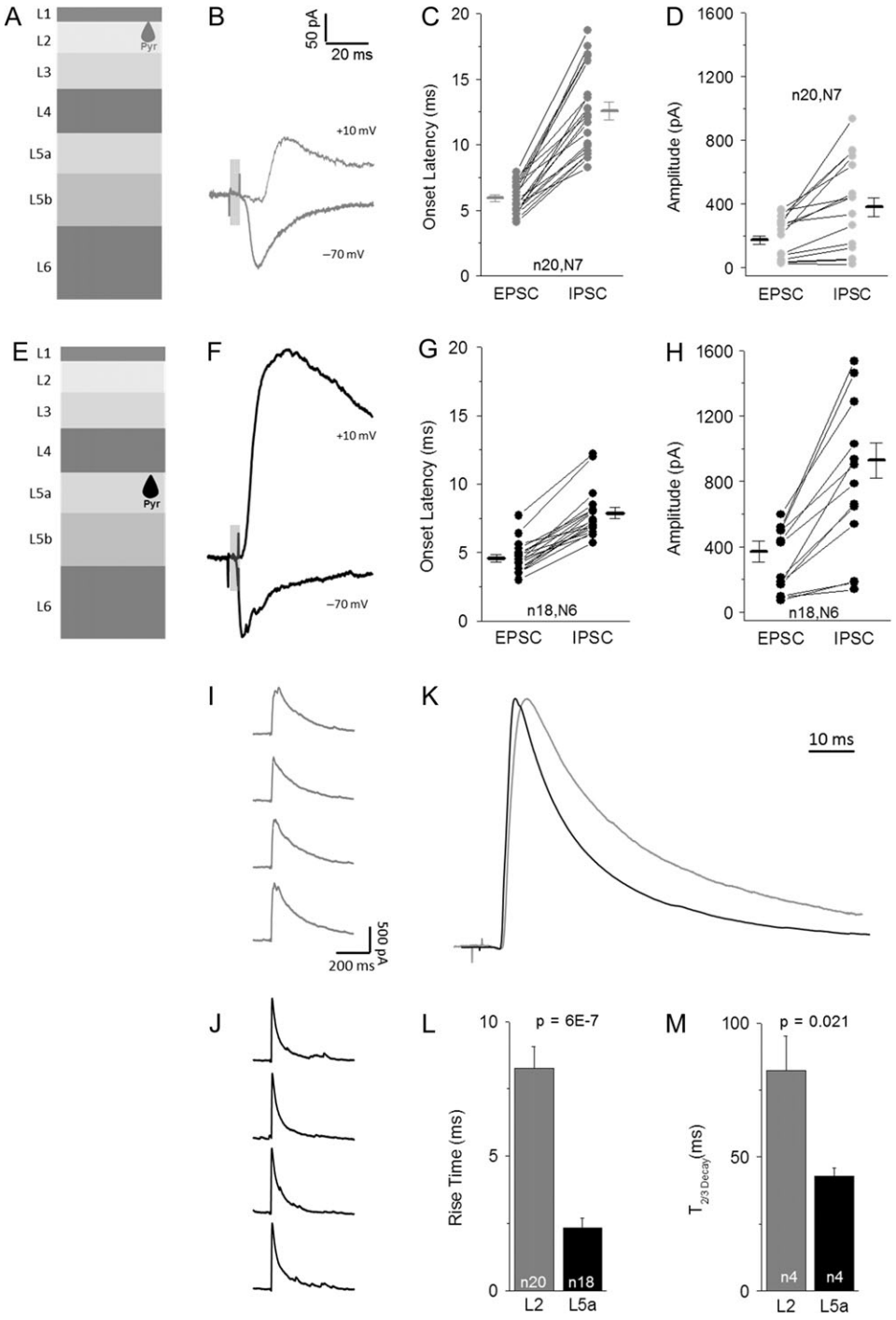


**Figure 4.** POm-evoked disynaptic inhibition is larger and faster in L5 Pyr neurons. (*A*) Schematic of L2 targeted Pyr neurons. (*B*) Example traces of average POm-evoked EPSC (−70 mV) and IPSC (+10 mV) responses. (*C*) Onset latency of POm-evoked EPSCs and IPSCs for L2 Pyr cells. Connected values for same cell. (*D*) Peak amplitude (<50 ms stim onset) of average EPSC and IPSC response for L2 Pyr neurons, connected values from same cell. (*E–H*) Example POm-evoked EPSC and IPSC (*F*), onset latency (*G*) and peak amplitude (*H*) for L5 Pyr neurons, same as *A–D*. (*I,J*) Consecutively recorded IPSCs in a L2 (*I*) and L5 (*J*) reveal kinetics and late-onset events. (*K*) Average of all L2 (gray) and L5 (black) IPSCs following minimal stimulation reveal differences in activation rate and duration of inhibition. Traces peak-scaled and aligned to rise. (*L,M*) Quantification of 10–90% rise time (*L*) and decay time (*M*, Time to 2/3 decay) for POm-evoked IPSCs is L2 (gray) and L5 (black) Pyr neurons. *Ns* are different in (*L*) and (*M*) due to inability to calculate decay with multiple pulses in some experiments.

are consistent with their origin in PV cells, which have a preferred perisomatic location for inputs (Kawaguchi and Kubota 1997). Although this does not rule out a contribution from 5HT3a neurons for disynaptic inhibition, it suggests that PV input is dominant.

As predicted from the pattern of direct synaptic input established in Figure 3, POm-evoked action potentials (APs) were never observed in SST-expressing neurons. In some cases, hyperpolarization of resting membrane potential was observed (Fig 5E; all cell mean −0.91 ± 0.9 mV; 3/6 cells), even though cells

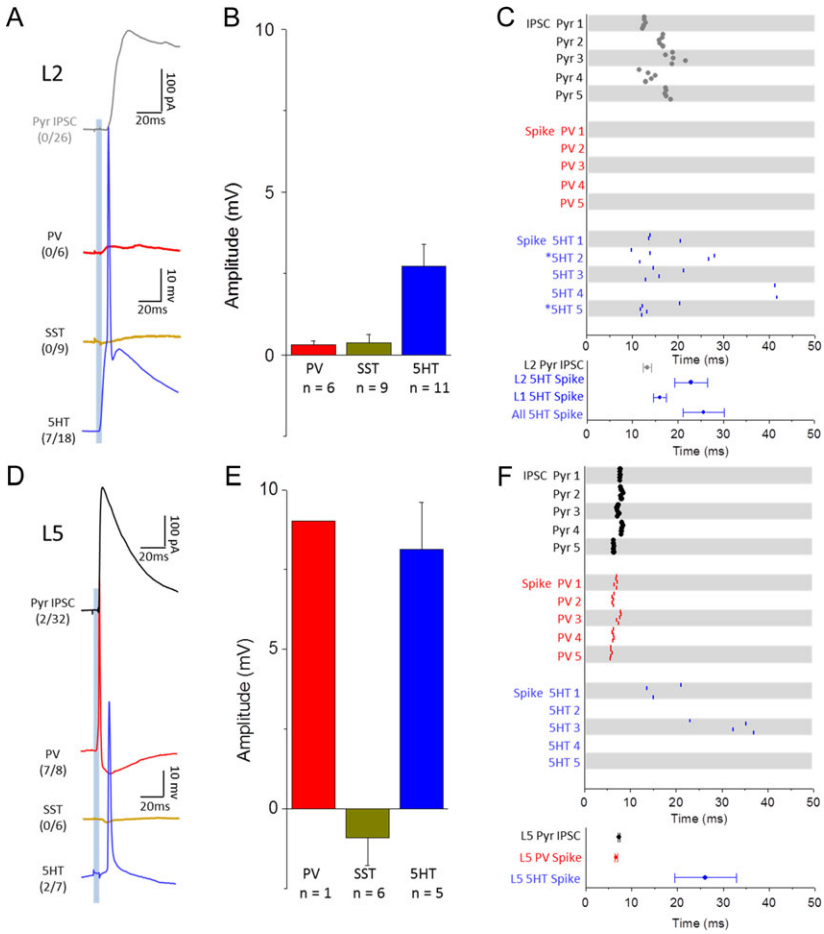


**Figure 5.** Feedforward inhibition is mediated by different inhibitory neuron populations in L2 and L5. (*A*) Example Pyr IPSC (black) compared to responses of PV (red), SST (yellow), and 5HT (blue) neuron populations in superficial layers following 5 ms optical stimulation of POm axons (single cell average 10 trials). Parentheses quantify number of cells that fired APs out of the total number recorded for each group. (*B*) Average peak EPSP (<50 ms post-stim) amplitude of non-spiking neurons for each inhibitory group. (*C*) Comparison of IPSC onset latency and spike timing for neuron populations in superficial layers. Raster (top) shows onset or spike peak time for 5 consecutive trials for 5 cells in each population. Asterisks (*) indicate 5HT neurons located in L1. Graph (bottom) quantifies average IPSC onset or spike peak latency across all neurons recorded in each population with 5HT neurons split by layer and in aggregate. (*D–F*) Same as (*A–C*) but for neurons in L5. Because all but 1 PV cell in L5 spiked in response to POm stimulation, the bar corresponding to L5 PV cell depolarization represents a single data point.

were resting near the Cl- reversal potential and thus these effects may be underestimated.

## Thalamocortical Response Transformations in L2 do not Involve Local PV Interneurons

The lack of direct synaptic input to PV neurons in L2, and the delay in the disynaptic IPSC in L2 Pyr cells suggested that the thalamocortical response transformation might be qualitatively different in this layer. To determine whether POm stimulation could drive firing in any of the 3 interneuron populations in superficial layers, targeted current-clamp recordings were carried out. Evoked spikes were aligned to IPSC onset for L2 Pyr neurons (Fig. 5A). POm stimulation never evoked an AP in any L2 PV (0/6) or SST neuron (0/9), and elicited small or negligible membrane potential depolarizations (Fig. 5A–C; PV cell mean 0.31 ± 0.1 mV; SST cell mean 0.36 ± 0.3 mV). In contrast, in 7/18 5HT3a neurons POm stimulation was sufficient to drive an AP, and the timing of these spikes was significantly delayed compared to evoked spikes in L5 PV neurons (spike latency L5 PV 6.6 ± 0.2 ms vs. L1/2 5HT3a 22.9 ± 3.6 ms). Of note, spike times for a given 5HT3a neuron were heterogeneous across stimulus trials, varying by as much as 10 ms, consistent with the large variability of IPSC onset observed for L2 Pyr neurons.

Overall, mean IPSC onset in L2 Pyr neurons occurred substantially later than L5 PV cell activity (Fig. 5C,F) and aligned with the earliest spikes in 5HT3a neurons (Fig. 5A,C), suggesting that L2 inhibition arises from neurons within this population. Consistent with this, previous studies have confirmed that superficial neurogliaform cells and, to a lesser extent, VIP-expressing neurons in L2 are synaptically connected to nearby Pyr neurons (Pfeffer et al. 2013; Jiang et al. 2015).

## POm-Driven Recurrent Activity is Layer-Specific

Our previous experiments employed recording conditions that isolated direct synaptic input from POm (in TTX and 4-AP), or in ACSF that enabled a single POm-driven spike in cortical neurons. To visualize a more complex sequence of recurrent network activity initiated by POm input and evaluate how different cell subtypes respond to this stimulus, we adjusted the bath solution to more closely mimic the composition of CSF in vivo (see Supplementary Table 2) (Sanchez-Vives and McCormick 2000; Shruti et al. 2008; Yassin et al. 2010; Urban-Ciecko et al. 2015).

Under these conditions, we observed occasional (<0.01 Hz) spontaneous membrane depolarizations similar to upstates, similar to those that have been described both in vitro and in vivo (Fanselow and Connors 2010; Beltramo et al. 2013; Neske et al. 2015).

Current-clamp recordings were carried out to examine how repetitive ChR2-mediated POm activation might drive recurrent activity across different cell types in L2 and L5 of the cortical column. POm stimulation was carried out at 12.5 Hz (5 pulses), a frequency that has been observed in POm neurons in awake animals (Urbain et al. 2015).

Consistent with EPSC measurements, L2 Pyr neurons showed a small EPSP, but firing was never evoked in these cells (Fig. 6B) even after long POm stimulus trains. These results are consistent with sparse activity that has been observed in L2 Pyr neurons, especially in somatosensory cortex (Barth and Poulet 2012; Yamashita et al. 2013; Jouhanneau et al. 2014). In some cases, repetitive POm stimulation was sufficient to drive prolonged depolarization that could last for several seconds (see Supplementary Fig. S3).

L2 PV neurons exhibited either no response or a small EPSP, with markedly less summation (Fig. 6C). On trials where very strong recurrent network activity was generated (see Supplementary Fig. S3 and Table 2) PV spiking was sometimes observed late in the stimulus train, and it could persist past the stimulation window (Fig. 6C,F). APs in L2 PV cells were never observed after the first few POm stimuli.

Previous studies have shown that both in vivo and in vitro, SST neurons throughout the neocortex exhibit tonic firing activity independent of synaptic input (Fanselow et al. 2008; Gentet et al. 2012; Urban-Ciecko et al. 2015). Interestingly, POm input initiated a hyperpolarization of resting membrane potential in SST neurons (Fig. 6D,J and Supplementary Fig. S3), remarkably consistent with sensory-evoked responses in this cell population in awake animals (Gentet et al. 2012). This hyperpolarization was sufficient to suppress spontaneous firing at the onset of the stimulation window. After an initial phase of firing suppression, mean SST firing frequency was modestly enhanced relative to baseline, though this increase was not significant (see Supplementary Fig. S3 and Table 2, baseline 6.0 ± 0.4 Hz, post-stim 8.0 ± 1.8 Hz, $P = 0.4$ paired t-test).

In contrast to the inability of POm stimulation to drive firing in other L2 cell types even when recurrent activity in the slice was enabled, 5HT3a neurons in superficial layers showed evoked firing, although the pattern and timing of spikes differed across cells. The 5HT3a neurons that exhibited POm-evoked firing were predominantly found in L2 or at the border between L1 and 2. As in Figure 6, spike times were heterogeneous even within a cell but were typically aligned to the stimulus pulse (Fig. 6E,F). In some cases, 5HT3a-cell firing persisted past the stimulus window, a phenomenon that was associated with strong recurrent activity as indicated by prolonged subthreshold depolarizations (see Supplementary Fig. S3 and Table 2).

VIP cells are a subset of 5HT3a-expressing GABAergic neurons (~38% of all 5HT3a neurons also showed VIP immunoreactivity in this 5HT3a-Cre line, similar to previous reports; Lee et al. 2013) and have been shown to synaptically inhibit SST neurons, a motif that is conserved across multiple brain areas including S1 (Lee et al. 2013; Pfeffer et al. 2013; Pi et al. 2013; Zhou et al. 2014; Jiang et al. 2015). Thus, it is possible that POm-evoked firing suppresses SST spontaneous activity at least in part through this disynaptic connection, from POm to VIP cell, to SST cell. To test whether POm can drive VIP neuron firing, fluorescently labeled L2 VIP neurons in S1 were targeted for recording in a VIP-Cre transgenic line (Taniguchi et al. 2011) with POm-targeted ChR2 expression. Optogenetic POm stimulation was carried out under recording conditions that enable recurrent activity (Fig. 7). Half of recorded VIP neurons (5/10) were strongly driven by POm stimulation across the stimulus window (Fig. 7B,C). Because VIP-inhibition of SST neurons has been well-documented, we conclude that this is a likely

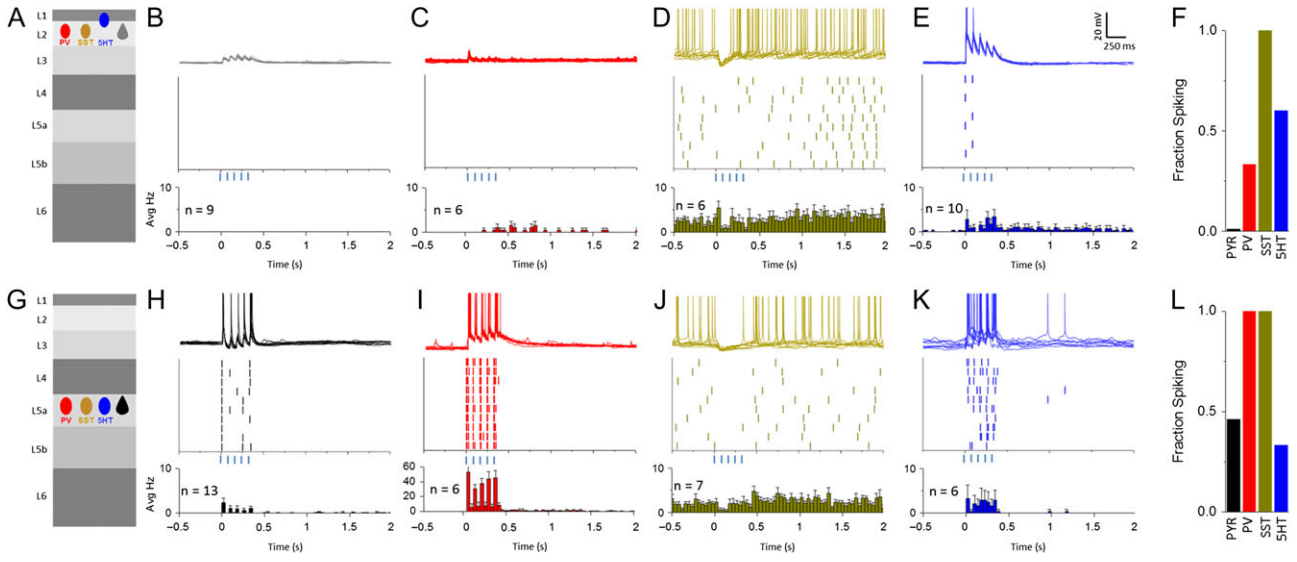


**Figure 6.** POm stimulation drives distinct patterns of recurrent activity in L2 and L5. (*A*) Schematic of cell type and layer of recorded population. (*B*) Top: 10 consecutive sweeps overlaid of L2 Pyr neuron in response to optical activations of POm in mACSF (For all: 5 pulses, 80 ms ISI). Middle: Raster plot showing spike peak times for example L2 Pyr cell. Bottom: Average peri-stimulus firing histogram for all L2 Pyr neurons recorded (For all: bin size 40 ms). Histogram includes cells that generated no APs. (*C–E*) As described in (*B*) for L2 PV (*C*), L2 SST (*D*), and L1/2 5HT neurons (*E*). SST neurons, if required, were manually adjusted to 48 ± 3 mV to evoke spontaneous APs and mimic in vivo membrane potential. (*F,L*) Bar graphs representing the fraction of neurons for each cell type that fired at least 1 AP during the stimulus window for each layer. (*G–K*) As described for (*A–E*) but in L5.

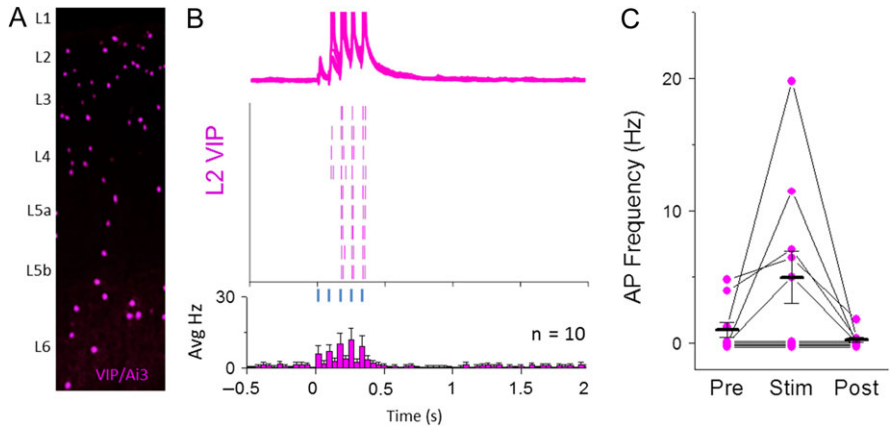


**Figure 7.** A subset of L2 VIP GABAergic neurons contribute to POm-evoked spiking pattern of L2 5HT neurons. (*A*) Schematic of VIP-expressing GABAergic neurons throughout a cortical column in S1 imaged with YFP fluorescence. (*B*) Top: Overlay of 10 consecutive POm-evoke responses in mACSF (5 light pulses, 80 ms ISI, max intensity). Middle: Raster plot showing spike times for 10 consecutive traces shown for sample cell. Bottom: average peri-stimulus firing histogram for all L2 VIP neurons recorded. (*C*) Firing rate quantification for 500 ms bins before, during, and after POm stimulation for all VIP neurons recorded. Cells with no evoked spikes are slightly offset for visibility.

pathway by which POm-driven hyperpolarization of SST neurons can occur.

Are VIP neurons the only source of POm-driven SST inhibition? 5HT3a neurons that exhibited non-VIP characteristics (L1 location or neurogliaform-like firing pattern) also were driven by POm stimulation, and these cells also inhibit SST neurons (Chittajallu et al. 2013; Jiang et al. 2013). Importantly, despite the reduction in inhibition from SST neurons during the stimulus period, POm activation was still insufficient to drive APs in L2 Pyr neurons under our recording conditions.

### Recurrent Activity in L5 Neural Subtypes is Dominated by Pyr and PV Neurons

POm stimulation was sufficient to drive firing in some L5a Pyr cells, where spikes occurred at short latency and with high fidelity. Although L5a Pyr neurons could fire after a single POm stimulus, this activity did not generate strong recurrent excitation in the circuit, and subsequent pulses were in fact less likely to trigger an AP.

These observations are consistent with POm-mediated, feedforward inhibition in the circuit, most likely from PV neurons that synapse densely onto neighboring L5 Pyr neurons (Packer and Yuste 2011; Avermann et al. 2012; Jiang et al. 2015; Pala and Petersen 2015). Indeed, ChR2-activation of POm afferents drove reliable and short-latency firing in L5 PV cells, and multiple spikes with very short inter-spike intervals (5–10 ms) were frequently observed after each light pulse (Fig. 6*I*,*L*). Prolonged activation after the stimulus window of L5 PV neurons was occasionally observed (2/6 cells).

L5 SST neurons showed similar behavior to those in L2: POm stimulation hyperpolarized these cells, suppressing spontaneous firing activity, especially during the early post-stimulus period (Fig. 6*J*, Supplementary Fig. S3). Similarly to L2, a minority of SST neurons displayed increased spontaneous firing after the POm stimulus window (see Supplementary Fig. S3 and Table 2; all cell means, baseline 4.9 ± 0.7 Hz, Post-stimulus 7.3 ± 0.8 Hz, $P = 0.740$ paired *t*-test).

The number of 5HT3a-expressing neurons in L5 is an order of magnitude lower than PV and SST neurons (Fig. 2*D*) (Lee et al. 2010), and it was often difficult to find more than 1 or 2 cells in a region with strong POm fiber labeling. However, as in L2, POm stimulation effectively drove firing in a subset (2/6) of 5HT3a neurons, and this firing was mainly restricted to the stimulus window although it was not tightly coupled to the stimulus itself (Fig. 6*F*,*L*). The sparseness of this cell population, the speed and reliability of POm-evoked firing in L5 PV cells, and the rapid IPSC onset observed in L5a Pyr cells suggest that inhibition from PV cells is likely to be a more potent regulator of L5a Pyr cell output.

## Discussion

Here we use a variety of electrophysiological methods to isolate, synapse by synapse and cell type by cell type, the earliest stages of thalamocortical response transformations. We show that a higher-order thalamic nucleus engages fundamentally distinct circuits in deep and superficial cortical layers, suggesting different modes of sensory processing in different lamina. Neurons in L5a are the main recipients of POm-driven activity, where Pyr neurons fire at short latency and with high precision maintained by fast, feedforward inhibition from local PV cells. In contrast, L2 Pyr neurons receive weak but direct POm input that summates over time due to delayed feedforward inhibition, likely from nearby 5HT3a cells. Remarkably, activation of POm inputs was sufficient to recapitulate dynamics of interneuron activity observed in awake animals in vivo, including weak excitation of L2 Pyr neurons, activation of putative 5HT3a neurons, and the sensory-evoked hyperpolarization of SST neurons (Gentet et al. 2012).

### Anatomical Versus Functional Connectivity of Thalamic Input

Our results both complement and constrain prior anatomical studies that attempt to define thalamocortical circuits (Woolsey and Van der Loos 1970; Koralek et al. 1988; Agmon et al. 1993; Meyer et al. 2010; Wimmer et al. 2010; Oberlaender et al. 2012). Dense reconstruction through electron microscopy images as well as rabies virus-mediated identification of presynaptic partners for a given cell type, seek to understand the function of thalamocortical inputs by defining the connection probabilities of specific neural subtypes. Although anatomical data can constrain hypotheses about neural computation, experimental

approaches that evaluate circuit properties through electrophysiological measurements will be required to determine how this architecture functions in real time.

For excitatory neurons, we found that direct synaptic input from POm onto excitatory neurons aligns with predictions based on axon-dendrite overlap and prior electrophysiological findings (Petreanu et al. 2009; Meyer et al. 2010). In contrast, functional inputs onto cortical inhibitory neurons showed cell-type specificity. In deep layers, POm provided direct input to PV- and 5HT3a-expressing interneurons but was not observed for SST neurons. In superficial layers, substantial direct input was only observed for 5HT3a-expressing interneurons and was absent for both PV and SST neurons. This layer-specific pattern of synaptic connectivity is surprising, since individual neurons in POm send axons to the cortex that branch and arborize in both L5a and L1 with the potential for substantial axon-dendrite overlap with SST and PV neurons in both layers (Ohno et al. 2012).

Our data suggest that SST neurons receive either weak or no input from POm, a finding that is on face inconsistent with a recent anatomical study using rabies virus to identify cell-type-specific presynaptic partners in somatosensory cortex (Wall et al. 2016). In this study, POm was identified as a presynaptic source of input to SST neurons from across the cortical column. How can this be reconciled with the current findings? First, our study focused on SST neurons in L2 and L5. In contrast, Wall et al examined inputs generally to SST neurons across the column. Because L4 SST neurons are molecularly and electrophysiologically distinct (McGarry et al. 2010) and may receive thalamic input (Tan et al. 2008; Hu and Agmon 2016), they may have been a major contributor driving apparent POm connectivity in rabies virus tracing studies.

In our assay, it is possible that POm synapses onto SST neurons were undercounted because they are strongly facilitating (Tan et al. 2008; Hu and Agmon 2016). However, ChR2-mediated release is typically very effective, even at synapses where release probability is low, and in our experiments even long stimulus trains did not reveal functional connections. Distal POm inputs to SST neurons might be anatomically present but electrophysiologically hard to detect; however, in most cases we did not observe even small or kinetically slow inputs following POm stimulation. It remains possible that there is state-dependent enhancement of weak POm inputs that could not be detected in our assay. Overall, functional data provided by electrophysiological measurements will be critical for understanding the circuit computations of different anatomical motifs.

## Common Principles for Thalamic Input to Granular and Infragranular Layers

POm input to L5 obeys wiring principles previously observed for VPM input to L4, with strong direct input to Pyr neurons, PV-expressing fast-spiking inhibitory neurons, and a sparse subpopulation of 5HT3a interneurons, and an absence of drive to SST neurons (Staiger et al. 1996; Cruikshank et al. 2007). Similar to VPM input to L4, POm activation can drive short latency, temporally precise APs in L5a Pyr neurons due to strong feedforward inhibition from PV interneurons. Parallel input to both excitatory and fast-spiking interneurons is believed to sharpen spatial and temporal resolution of sensory responses, and has been observed for thalamic input to L4 and non-granular layers in different regions of sensory neocortex (Gabernet et al. 2005; Cruikshank et al. 2007, 2012; Schiff and Reyes 2012; Kloc and Maffei 2014; Delevich et al. 2015; Ji et al. 2016).

VPM and POm have comparable levels of firing during wakefulness and whisking (Urbain et al. 2015), indicating that these inputs are simultaneously active. Although we found that POm stimulation elicited the strongest depolarization in L2 and L5, excitatory neurons in all layers showed some response, similar to what has been inferred for VPM synapses (Meyer et al. 2010; Oberlaender et al. 2012). Thus, neocortical neurons, particularly those in L5, are in a position to receive direct convergent input from both thalamic nuclei (Meyer et al. 2010; Mease et al. 2016). Because the thalamic wiring principles for different cell types are conserved between L4 and L5, we predict that simultaneous activation of VPM and POm will have qualitatively similar effects, i.e., forcing temporal fidelity of spikes in L5 Pyr neurons to a stimulus.

## POm-Activation Drives Progressive Depolarization in L2 Pyr Neurons

In striking contrast to L5a, we found that POm was insufficient to drive APs in L2 Pyr neurons, despite the absence of local PV inhibition and even with EPSP summation during repetitive POm stimulation. The lack of firing is particularly notable because ChR2-stimulation of POm afferents is synchronous, unlike what might occur during normal sensation, and provides an upper bound for how strong this input can be.

Our findings are consistent with observations that L2 neurons fire sparsely during whisker stimulation in vivo (de Kock et al. 2007; Barth and Poulet 2012; Chen et al. 2013; Yamashita et al. 2013). What might be the right conditions to drive firing in L2 Pyr cells? In vivo, both POm and VPM are simultaneously active (Urbain et al. 2015), and this combined input (direct from POm and indirect via L4 from VPM), especially with a more complex sensory stimulus, might be sufficient to drive spikes in some neurons. In addition, weak and delayed inhibition from 5HT3a neurons—in combination with the silencing of SST interneurons—might enable L2 Pyr neurons to be particularly sensitive to delayed and convergent input from other brain areas, such as M1 or S2, or ascending inputs within the column (Feldmeyer et al. 2013; Kinnischtzke et al. 2014; Urban-Ciecko et al. 2015). Indeed, L2 neurons show considerable experience-dependent plasticity in vivo (Fox 1992; Glazewski and Fox 1996; Clem and Barth 2006; Benedetti et al. 2009; Wen and Barth 2011; Gambino et al. 2014; Margolis et al. 2014), a property that might be related to their ability to associate inputs arriving from multiple sources.

## Cell-Type-Specific Dynamics are Similar to In Vivo Recordings

In vivo, targeted whole-cell recordings of identified neuronal subtypes have revealed characteristic sensory-evoked responses in superficial layers of barrel S1 and other cortical sensory areas (Gentet et al. 2012; Mesik et al. 2015). For example, whisker stimulation elicits depolarization but not spiking in L2 Pyr cells, hyperpolarization in SST cells, and delayed firing in subsets of 5HT3a cells. Remarkably, our data indicate that the essential circuitry to generate previously observed, cell-type-specific patterns of activity can be retained in a reduced preparation and do not require input from other brain areas.

SST inhibition by VIP-expressing interneurons is a common connectivity motif that has been observed in multiple brain areas, including S1 (Lee et al. 2013; Pfeffer et al. 2013; Pi et al.

2013; Fu et al. 2014; Zhang et al. 2014; Jiang et al. 2015). We found that POm activation could drive firing in 5HT3a neurons, a large and heterogeneous class of inhibitory neurons that includes VIP cells. Indeed, optogenetic POm stimulation evoked firing in VIP neurons, providing a mechanism by which POm-driven SST hyperpolarization might occur. However, POm stimulation also evoked firing in L1 5HT3a neurons, where VIP cells are not observed (Olàh et al. 2007; Jiang et al. 2013, 2015; Lee et al. 2013). Thus, there may be multiple pathways by which thalamic input can suppress SST activity.

Even within defined subpopulations of 5HT3a neurons, such as L2 VIP neurons or L1 5HT3a neurons, synaptic and firing responses were still heterogeneous. These properties are consistent with the anatomical and electrophysiological diversity observed in this general cell class (Lee et al. 2010; Prönneke et al. 2015) and support the idea that there may be multiple functionally distinct subpopulations with unique roles in shaping cortical responses. Interestingly, the preliminary evidence for input from primary thalamic nuclei, such as VPM or the lateral geniculate nucleus, to VIP neurons is inconsistent across cortical regions (Staiger et al. 1996; Ji et al. 2016; Wall et al. 2016). It will be critical to determine how long-range and local circuits target specific anatomically and genetically defined subpopulations of 5HT3a neurons to understand the effect of this population on cortical processing.

POm-mediated SST silencing was observed in both superficial and deep layers, despite the scarcity of 5HT3a neurons in granular and infragranular layers. It is possible that translaminar inhibition from superficial VIP neurons or NGF neurons in L2 might contribute to POm-evoked SST silencing in deep layers (Lee et al. 2010; Prönneke et al. 2015), and translaminar synaptic connections to SST cells have been documented (Jiang et al. 2015). A reduction in the tonic firing of SST neurons, observed in vivo and also in our experimental preparation, may be important for stimulus detection and circuit plasticity.

In vivo, POm neurons fire at 10–15 Hz during active touch, and optogenetic activation of these inputs trigger prolonged firing in the neocortex when paired with whisker stimulation (Urbain et al. 2015; Mease et al. 2016). In these experiments even transient optogenetic stimulation of POm alone was sufficient to drive prolonged firing in L5 neurons. Although repetitive POm fiber activation in acute brain slices cannot capture all properties of this corticothalamic loop (Cruikshank et al. 2010; Groh et al. 2014; Crandall et al. 2015), the earliest sequence of synaptic input and spikes are likely to be conserved. POm stimulation at naturalistic frequencies was sufficient to drive prolonged network activity in both L2 and L5 which could last hundreds of milliseconds after the final stimulus. While additional long-range pathways may also contribute to the delayed activity observed in vivo, our results indicate that some of this activity must be generated by local circuit interactions.

### Future Directions

Results presented here showcase the ability of in vitro methods to replicate complex, in vivo dynamics and attribute them to specific long-range inputs and cell populations. This detailed and dynamic analysis of individual long-range inputs will help build conceptual bridges between precise cell-type-specific connectivity maps and the complex dynamics observed during active sensation and behavior in vivo (Fino and Yuste 2011; Gentet et al. 2012; Pfeffer et al. 2013; Pi et al. 2013; Jiang et al. 2015; Pala and Petersen 2015). Further, these methods are modular and can be easily expanded to investigate the interplay of multiple, precisely controlled long-range inputs using multi-channel optogenetic strategies (Klapoetke et al. 2014).

Additionally, the activation of VIP interneurons, relief of SST inhibition, and the absence of strong PV inhibition in L2 with POm activation may have important implications for plasticity both of thalamocortical inputs and intracortical circuits (Fu et al. 2015). Understanding what information is conveyed by POm activity, dissecting how multiple thalamic and cortical pathways converge on individual neurons and probing the role of POm in plasticity and ensemble formation will be critical for advancing our understanding of the algorithm by which cortical circuitry transforms sensory input.

## Supplementary Material

Supplementary material is available at *Cerebral Cortex* online.

## Funding

This work was supported by the National Institutes of Health (NIH DA0171088 and NS088958 to A.L.B.); the McKnight Foundation to A.L.B.; and the Carnegie Foundation to N.J.A.

## Notes

Special thanks to Joanne Steinmiller for expert animal care, Rogan Grant for technical assistance, and D.J. Braiser, James Poulet, and members of the Barth lab for helpful comments on the manuscript. *Conflict of Interest*: None declared.

## References

Agmon A, Connors BW. 1992. Correlation between intrinsic firing patterns and thalamocortical synaptic responses of neurons in mouse barrel cortex. J Neurosci. 12:319–329.

Agmon A, Yang LT, O'Dowd DK, Jones EG. 1993. Organized growth of thalamocortical axons from the deep tier of terminations into layer IV of developing mouse barrel cortex. J Neurosci. 13:5365–5382.

Ahissar E, Sosnik R, Bagdasarian K, Haidarliu S. 2001. Temporal frequency of whisker movement. II. Laminar organization of cortical representations. J Neurophysiol. 86:354–367.

Avermann M, Tomm C, Mateo C, Gerstner W, Petersen CCH. 2012. Microcircuits of excitatory and inhibitory neurons in layer 2/3 of mouse barrel cortex. J Neurophysiol. 107: 3116–3134.

Barth AL, Poulet JFA. 2012. Experimental evidence for sparse firing in the neocortex. Trends Neurosci. 35:345–355.

Beltramo R, D'Urso G, Maschio MD, Farisello P, Bovetti S, Clovis Y, Lassi G, Tucci V, De Pietri Tonelli D, Fellin T. 2013. Layer-specific excitatory circuits differentially control recurrent network dynamics in the neocortex. Nat Med. 16:1–10.

Benedetti BL, Glazewski S, Barth AL. 2009. Reliable and precise neuronal firing during sensory plasticity in superficial layers of primary somatosensory cortex. J Neurosci. 29: 11817–11827.

Bock DD, Lee W-CA, Kerlin AM, Andermann ML, Hood G, Wetzel AW, Yurgenson S, Soucy ER, Kim HS, Reid RC. 2011. Network anatomy and in vivo physiology of visual cortical neurons. Nature. 471:177–182.

Bureau I, Von Saint Paul F, Svoboda K. 2006. Interdigitated paralemniscal and lemniscal pathways in the mouse barrel cortex. PLoS Biol. 4:2361–2371.

Chen JL, Carta S, Soldado-Magraner J, Schneider BL, Helmchen F. 2013. Behaviour-dependent recruitment of long-range projection neurons in somatosensory cortex. Nature. 499: 336–340.

Chen JL, Margolis DJ, Stankov A, Sumanovski LT, Schneider BL, Helmchen F. 2015. Pathway-specific reorganization of projection neurons in somatosensory cortex during learning. Nat Neurosci. 18:1101–1108.

Chittajallu R, Pelkey KA, McBain CJ. 2013. Neurogliaform cells dynamically regulate somatosensory integration via synapse-specific modulation. Nat Neurosci. 16:13–15.

Chmielowska J, Carvell GE, Simons DJ. 1989. Spatial organization of thalamocortical and corticothalamic projection systems in the rat SmI barrel cortex. J Comp Neurol. 285:325–338.

Clem RL, Barth A. 2006. Pathway-specific trafficking of native AMPARs by in vivo experience. Neuron. 49:663–670.

Constantinople CM, Bruno RM. 2013. Deep cortical layers are activated directly by thalamus. Science. 340:1591–1594.

Crandall SR, Cruikshank SJ, Connors BW. 2015. A corticothalamic switch: controlling the thalamus with dynamic synapses. Neuron. 86:768–782.

Cruikshank SJ, Ahmed OJ, Stevens TR, Patrick SL, Gonzalez AN, Elmaleh M, Connors BW. 2012. Thalamic control of layer 1 circuits in prefrontal cortex. J Neurosci. 32:17813–17823.

Cruikshank SJ, Lewis TJ, Connors BW. 2007. Synaptic basis for intense thalamocortical activation of feedforward inhibitory cells in neocortex. Nat Neurosci. 10:462–468.

Cruikshank SJ, Urabe H, Nurmikko AV, Connors BW. 2010. Pathway-specific feedforward circuits between thalamus and neocortex revealed by selective optical stimulation of axons. Neuron. 65:230–245.

de Kock CPJ, Bruno RM, Spors H, Sakmann B. 2007. Layer- and cell-type-speci c suprathreshold stimulus representation in rat primary somatosensory cortex. Society. 1:139–154.

Delevich K, Tucciarone J, Huang ZJ, Li B. 2015. The mediodorsal thalamus drives feedforward inhibition in the anterior cingulate cortex via parvalbumin interneurons. J Neurosci. 35: 5743–5753.

Diamond ME, Armstrong-James M, Budway MJ, Ebner FF. 1992. Somatic sensory responses in the rostral sector of the posterior group (POm) and in the ventral posterior medial nucleus (VPM) of the rat thalamus: dependence on the barrel field cortex. J Comp Neurol. 319:66–84.

Fanselow EE, Connors BW. 2010. The roles of somatostatin-expressing (GIN) and fast-spiking inhibitory interneurons in UP-DOWN states of mouse neocortex. J Neurophysiol. 104: 596–606.

Fanselow EE, Richardson KA, Connors BW. 2008. Selective, state-dependent activation of somatostatin-expressing inhibitory interneurons in mouse neocortex. J Neurophysiol. 100:2640–2652.

Feldmeyer D, Brecht M, Helmchen F, Petersen CCH, Poulet JFA, Staiger JF, Luhmann HJ, Schwarz C. 2013. Barrel cortex function. Prog Neurobiol. 103:3–27.

Fino E, Yuste R. 2011. Dense inhibitory connectivity in neocortex. Neuron. 69:1188–1203.

Fox K. 1992. A critical period for experience-dependent synaptic plasticity in rat barrel cortex. J Neurosci. 12:1826–1838.

Fu Y, Kaneko M, Tang Y, Alvarez-Buylla A, Stryker MP. 2015. A cortical disinhibitory circuit for enhancing adult plasticity. Elife. 2015:1–12.

Fu Y, Tucciarone JM, Espinosa JS, Sheng N, Darcy DP, Nicoll RA, Huang ZJ, Stryker MP. 2014. A cortical circuit for gain control by behavioral state. Cell. 156:1139–1152.

Gabernet L, Jadhav SP, Feldman DE, Carandini M, Scanziani M. 2005. Somatosensory integration controlled by dynamic thalamocortical feed-forward inhibition. Neuron. 48:315–327.

Gambino F, Pagès S, Kehayas V, Baptista D, Tatti R, Carleton A, Holtmaat A. 2014. Sensory-evoked LTP driven by dendritic plateau potentials in vivo. Nature. 515:116–119.

Gentet LJ, Kremer Y, Taniguchi H, Huang ZJ, Staiger JF, Petersen CC. 2012. Unique functional properties of somatostatin-expressing GABAergic neurons in mouse barrel cortex. Nat Neurosci. 15:607–612.

Glazewski S, Fox K. 1996. Time course of experience-dependent synaptic potentiation and depression in barrel cortex of adolescent rats. J Neurophysiol. 75:1714–1729.

Gong S, Doughty M, Harbaugh CR, Cummins A, Hatten ME, Heintz N, Gerfen CR. 2007. Targeting Cre recombinase to specific neuron populations with bacterial artificial chromosome constructs. J Neurosci. 27:9817–9823.

Groh A, Bokor H, Mease RA, Plattner VM, Hangya B, Stroh A, Deschenes M, Acsády L. 2014. Convergence of cortical and sensory driver inputs on single thalamocortical cells. Cereb Cortex. 24:3167–3179.

Hangya B, Pi HJ, Kvitsiani D, Ranade SP, Kepecs A. 2014. From circuit motifs to computations: mapping the behavioral repertoire of cortical interneurons. Curr Opin Neurobiol. 26: 117–124.

Harris KD, Mrsic-Flogel TD. 2013. Cortical connectivity and sensory coding. Nature. 503:51–58.

Harris KD, Shepherd GMG. 2015. The neocortical circuit: themes and variations. Nat Neurosci. 18:170–181.

Hippenmeyer S, Vrieseling E, Sigrist M, Portmann T, Laengle C, Ladle DR, Arber S. 2005. A developmental switch in the response of DRG neurons to ETS transcription factor signaling. PLoS Biol. 3:0878–0890.

Hu H, Agmon A. 2016. Differential excitation of distally versus proximally targeting cortical interneurons by unitary thalamocortical bursts. J Neurosci. 36:6906–6916.

Ji XY, Zingg B, Mesik L, Xiao Z, Zhang LI, Tao HW. 2016. Thalamocortical innervation pattern in mouse auditory and visual cortex: laminar and cell-type specificity. Cereb Cortex. 26:2612–2625.

Jiang X, Shen S, Cadwell CR, Berens P, Sinz F, Ecker AS, Patel S, Tolias AS. 2015. Principles of connectivity among morphologically defined cell types in adult neocortex. Science. 350: aac9462.

Jiang X, Wang G, Lee AJ, Stornetta RL, Zhu JJ. 2013. The organization of two new cortical interneuronal circuits. Nat Neurosci. 16:210–218.

Jouhanneau JS, Ferrarese L, Estebanez L, Audette NJ, Brecht M, Barth AL, Poulet JFA. 2014. Cortical fos GFP expression reveals broad receptive field excitatory neurons targeted by POm. Neuron. 84:1065–1078.

Kawaguchi Y, Kubota Y. 1997. GABAergic cell subtypes and their synaptic connections in rat frontal cortex. Cereb Cortex. 7:476–486.

Kinnischtzke AK, Simons DJ, Fanselow EE. 2014. Motor cortex broadly engages excitatory and inhibitory neurons in somatosensory barrel cortex. Cereb Cortex. 24:2237–2248.

Klapoetke NC, Murata Y, Kim SS, Pulver SR, Birdsey-Benson A, Cho YK, Morimoto TK, Chuong AS, Carpenter EJ, Tian Z, et al. 2014. Independent optical excitation of distinct neural populations. Nat Methods. 11:338–346.

Kloc M, Maffei A. 2014. Target-specific properties of thalamocortical synapses onto layer 4 of mouse primary visual cortex. J Neurosci. 34:15455–15465.

Koralek KA, Jensen KF, Killackey HP. 1988. Evidence for two complementary patterns of thalamic input to the rat somatosensory cortex. Brain Res. 463:346–351.

Lee S, Hjerling-Leffler J, Zagha E, Fishell G, Rudy B. 2010. The largest group of superficial neocortical GABAergic interneurons expresses ionotropic serotonin receptors. J Neurosci. 30: 16796–16808.

Lee S, Kruglikov I, Huang ZJ, Fishell G, Rudy B. 2013. A disinhibitory circuit mediates motor integration in the somatosensory cortex. Nat Neurosci. 16:1662–1670.

Lee WA, Bonin V, Reed M, Graham BJ, Hood G, Glattfelder K, Reid RC. 2016. Anatomy and function of an excitatory network in the visual cortex. Nature. 532:1–18.

Lefort S, Tomm C, Floyd Sarria JC, Petersen CCH. 2009. The excitatory neuronal network of the C2 barrel column in mouse primary somatosensory cortex. Neuron. 61:301–316.

Margolis DJ, Lütcke H, Helmchen F. 2014. Microcircuit dynamics of map plasticity in barrel cortex. Curr Opin Neurobiol. 24: 76–81.

McGarry LM, Packer AM, Fino E, Nikolenko V, Sippy T, Yuste R. 2010. Quantitative classification of somatostatin-positive neocortical interneurons identifies three interneuron subtypes. Front Neural Circuits. 4:12.

Mease RA, Metz M, Groh A. 2016. Cortical sensory responses are enhanced by the higher-order thalamus. Cell Rep. 14: 208–215.

Mesik L, Ma W-P, Li L-Y, Ibrahim LA, Huang ZJ, Zhang LI, Tao HW. 2015. Functional response properties of VIP-expressing inhibitory neurons in mouse visual and auditory cortex. Front Neural Circuits. 9:22.

Meyer HS, Wimmer VC, Hemberger M, Bruno RM, De Kock CPJ, Frick A, Sakmann B, Helmstaedter M. 2010. Cell type-specific thalamic innervation in a column of rat vibrissal cortex. Cereb Cortex. 20:2287–2303.

Miller KD. 2016. Canonical computations of cerebral cortex. Curr Opin Neurobiol. 37:75–84.

Miyoshi G, Hjerling-leffler J, Karayannis T, Sousa VH, Butt JB, Battiste J, Johnson JE, Machold RP, Fishell G. 2010. Genetic fate mapping reveals that the caudal ganglionic eminence produces a large and diverse population of superficial cortical interneurons. J Neurosci. 30:1582–1594.

Neske GT, Patrick SL, Connors BW. 2015. Contributions of diverse excitatory and inhibitory neurons to recurrent network activity in cerebral cortex. J Neurosci. 35:1089–1105.

Oberlaender M, De Kock CPJ, Bruno RM, Ramirez A, Meyer HS, Dercksen VJ, Helmstaedter M, Sakmann B. 2012. Cell type-specific three-dimensional structure of thalamocortical circuits in a column of rat vibrissal cortex. Cereb Cortex. 22: 2375–2391.

Ohno S, Kuramoto E, Furuta T, Hioki H, Tanaka YR, Fujiyama F, Sonomura T, Uemura M, Sugiyama K, Kaneko T. 2012. A morphological analysis of thalamocortical axon fibers of rat posterior thalamic nuclei: a single neuron tracing study with viral vectors. Cereb Cortex. 22:2840–2857.

Olàh S, Komlòsi G, Szabadics J, Varga C, Tòth E, Barzò P, Tamas G, Barzò P. 2007. Output of neurogliaform cells to various neuron types in the human and rat cerebral cortex. Front Neural Circuits. 1:1–7.

Packer AM, Yuste R. 2011. Dense, unspecific connectivity of neocortical parvalbumin-positive interneurons: a canonical microcircuit for inhibition? J Neurosci. 31:13260–13271.

Pala A, Petersen CCH. 2015. Invivo measurement of cell-type-specific synaptic connectivity and synaptic transmission in layer 2/3 mouse barrel cortex. Neuron. 85:68–76.

Petreanu L, Huber D, Sobczyk A, Svoboda K. 2007. Channelrhodopsin-2-assisted circuit mapping of long-range callosal projections. Nat Neurosci. 10:663–668.

Petreanu L, Mao T, Sternson SM, Svoboda K. 2009. The subcellular organization of neocortical excitatory connections. Nature. 457:1142–1145.

Pfeffer CK, Xue M, He M, Huang ZJ, Scanziani M. 2013. Inhibition of inhibition in visual cortex: the logic of connections between molecularly distinct interneurons. Nat Neurosci. 16:1068–1076.

Pi H-J, Hangya B, Kvitsiani D, Sanders JI, Huang ZJ, Kepecs A. 2013. Cortical interneurons that specialize in disinhibitory control. Nature. 503:521–524.

Porter JT, Johnson CK, Agmon A. 2001. Diverse types of interneurons generate thalamus-evoked feedforward inhibition in the mouse barrel cortex. J Neurosci. 21:2699–2710.

Prönneke A, Scheuer B, Wagener RJ, Möck M, Witte M, Staiger JF. 2015. Characterizing VIP neurons in the barrel cortex of VIPcre/tdTomato mice reveals layer-specific differences. Cereb Cortex. 25:4854–4868.

Purushothaman G, Marion R, Li K, Casagrande VA. 2012. Gating and control of primary visual cortex by pulvinar. Nat Neurosci. 15:905–912.

Roth MM, Dahmen JC, Muir DR, Imhof F, Martini FJ, Hofer SB. 2016. Thalamic nuclei convey diverse contextual information to layer 1 of visual cortex. Nat Neurosci. 19:299–307.

Rudy B, Fishell G, Lee S, Hjerling-Leffler J. 2011. Three groups of interneurons account for nearly 100% of neocortical GABAergic neurons. Dev Neurobiol. 71:45–61.

Sanchez-Vives MV, McCormick DA. 2000. Cellular and network mechanisms of rhythmic recurrent activity in neocortex. Nat Neurosci. 3:1027–1034.

Schiff ML, Reyes AD. 2012. Characterization of thalamocortical responses of regular-spiking and fast-spiking neurons of the mouse auditory cortex in vitro and in silico. J Neurophysiol. 107:1476–1488.

Sherman SM. 2016. Thalamus plays a central role in ongoing cortical functioning. Nat Neurosci. 16:533–541.

Shruti S, Clem RL, Barth AL. 2008. A seizure-induced gain-of-function in BK channels is associated with elevated firing activity in neocortical pyramidal neurons. Neurobiol Dis. 30: 323–330.

Silberberg G, Markram H. 2007. Disynaptic inhibition between neocortical pyramidal cells mediated by martinotti cells. Neuron. 53:735–746.

Staiger JF, Zilles K, Freund TF. 1996. Innervation of VIP-immunoreactive neurons by the ventroposteromedial thalamic nucleus in the barrel cortex of the rat. J Comp Neurol. 367:194–204.

Swadlow HA, Gusev AG. 2002. Receptive-field construction in cortical inhibitory interneurons. Nat Neurosci. 5:403–404.

Tan Z, Hu H, Huang ZJ, Agmon A. 2008. Robust but delayed thalamocortical activation of dendritic-targeting inhibitory interneurons. Proc Natl Acad Sci USA. 105:2187–2192.

Taniguchi H, He M, Wu P, Kim S, Paik R, Sugino K, Kvitsani D, Fu Y, Lu J, Lin Y, et al. 2011. A resource of cre driver lines for genetic targeting of GABAergic neurons in cerebral cortex. Neuron. 71:995–1013.

Urbain N, Salin PA, Libourel PA, Comte JC, Gentet LJ, Petersen CCH. 2015. Whisking-related changes in neuronal firing and membrane potential dynamics in the somatosensory thalamus of awake mice. Cell Rep. 13:647–656.

Urban-Ciecko J, Fanselow EE, Barth AL. 2015. Neocortical somatostatin neurons reversibly silence excitatory transmission via GABAb receptors. Curr Biol. 25:722–731.

Vélez-Fort M, Rousseau CV, Niedworok CJ, Wickersham IR, Rancz EA, Brown APY, Strom M, Margrie TW. 2014. The stimulus selectivity and connectivity of layer six principal cells reveals cortical microcircuits underlying visual processing. Neuron. 83:1431–1443.

Viaene AN, Petrof I, Sherman SM. 2011. Properties of the thalamic projection from the posterior medial nucleus to primary and secondary somatosensory cortices in the mouse. Proc Natl Acad Sci. 108:18156–18161.

Wall NR, De La Parra M, Sorokin JM, Taniguchi H, Huang ZJ, Callaway EM. 2016. Brain-wide maps of synaptic input to cortical interneurons. J Neurosci. 36:4000–4009.

Wen JA, Barth AL. 2011. Input-specific critical periods for experience-dependent plasticity in layer 2/3 pyramidal neurons. Animals. 31:4456–4465.

Wimmer VC, Bruno RM, De Kock CPJ, Kuner T, Sakmann B. 2010. Dimensions of a projection column and architecture of VPM and POm axons in rat vibrissal cortex. Cereb Cortex. 20: 2265–2276.

Woolsey TA, Van der Loos H. 1970. The structural organization of layer IV in the somatosensory region (S I) of mouse cerebral cortex. The description of a cortical field composed of discrete cytoarchitectonic units. Brain Res. 17:205–242.

Xu H, Jeong HY, Tremblay R, Rudy B. 2013. Neocortical somatostatin-expressing GABAergic interneurons disinhibit the thalamorecipient layer 4. Neuron. 77:155–167.

Xue M, Atallah BV, Scanziani M. 2014. Equalizing excitation-inhibition ratios across visual cortical neurons. Nature. 511: 596–600.

Yamashita T, Pala A, Pedrido L, Kremer Y, Welker E, Petersen CCH. 2013. Membrane potential dynamics of neocortical projection neurons driving target-specific signals. Neuron. 80:1477–1490.

Yassin L, Benedetti BL, Jouhanneau JS, Wen JA, Poulet JFA, Barth AL. 2010. An embedded subnetwork of highly active neurons in the neocortex. Neuron. 68:1043–1050.

Yu C, Derdikman D, Haidarliu S, Ahissar E. 2006. Parallel thalamic pathways for whisking and touch signals in the rat. PLoS Biol. 4:e124.

Yu C, Horev G, Rubin N, Derdikman D, Haidarliu S, Ahissar E. 2015. Coding of object location in the vibrissal thalamocortical system. Cereb Cortex. 25:563–577.

Yuste R. 2015. From the neuron doctrine to neural networks. Nat Rev Neurosci. 16:487–497.

Zhang S, Xu M, Kamigaki T, Phong Hoang Do J, Chang W-C, Jenvay S, Miyamichi K, Luo L, Dan Y. 2014. Long-range and local circuits for top-down modulation of visual cortex processing. Science. 345:660–665.

Zhou M, Liang F, Xiong XR, Li L, Li H, Xiao Z, Tao HW, Zhang LI. 2014. Scaling down of balanced excitation and inhibition by active behavioral states in auditory cortex. Nat Neurosci. 17: 841–850.